

---

# Late-Constraint Diffusion Guidance for Controllable Image Synthesis

---

Chang Liu<sup>1</sup>, Dong Liu<sup>1\*</sup>

<sup>1</sup>University of Science and Technology of China  
lc980413@mail.ustc.edu.cn, dongeliu@ustc.edu.cn

## Abstract

Diffusion models, either with or without text condition, have demonstrated impressive capability in synthesizing photorealistic images given a few or even no words. These models may not fully satisfy user need, as normal users or artists intend to control the synthesized images with specific guidance, like overall layout, color, structure, object shape, and so on. To adapt diffusion models for controllable image synthesis, several methods have been proposed to incorporate the required conditions as regularization upon the intermediate features of the diffusion denoising network. These methods, known as *early-constraint* ones in this paper, have difficulties in handling multiple conditions with a single solution. They intend to train separate models for each specific condition, which require much training cost and result in non-generalizable solutions. To address these difficulties, we propose a new approach namely *late-constraint*: we leave the diffusion networks unchanged, but constrain its output to be aligned with the required conditions. Specifically, we train a lightweight condition adapter to establish the correlation between external conditions and internal representations of diffusion models. During the iterative denoising process, the conditional guidance is sent into corresponding condition adapter to manipulate the sampling process with the established correlation. We further equip the introduced late-constraint strategy with a timestep resampling method and an early stopping technique, which boost the quality of synthesized image meanwhile complying with the guidance. Using the proposed method, we manage to perform image synthesis upon multiple conditions at the training cost of several hours on a single 3090 GPU. Our method outperforms the existing early-constraint methods and demonstrates multiple applications with its plausible generalization ability and flexible controllability.

## 1 Introduction

Recently, diffusion model has come into prominence in the field of image synthesis. With the enhancement of multimodal learning [46, 11, 47], text-to-image diffusion model [49, 24, 52, 42, 17, 1, 31, 6, 16, 30, 37] has revealed plausible generation ability in numerous tasks. Such model is capable of producing photorealistic results given a few words of description or even none, which has revealed great potentials for inspiring and creative applications.

Nevertheless, text prompts could still be limited during user interfaces. It could be ambiguous if used to describe structural information as guidance, *e.g.*, layout, structure, object position, and so on. Such limitations motivate several methods [66, 41], to introduce more precise control upon diffusion models. As is shown Fig. 1, these methods, known as *early-constraint* ones in this paper, implement condition-specific encoders to regularize the intermediate layers of diffusion denoising networks. However, learning the process of such intra-manipulation requires much resources to

---

\*Corresponding author.

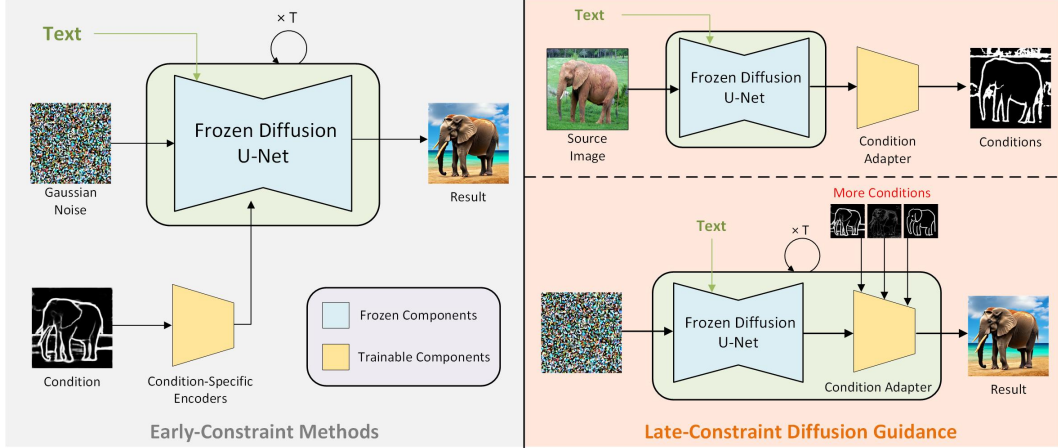


Figure 1: Compared to existing *early-constraint* solutions, we present *Late-Constraint Diffusion Guidance (LCDG)*, to provide guidance for diffusion models externally meanwhile keeping the diffusion U-Net unchanged.

implement. Furthermore, such techniques are confined as one-for-one solutions, which sacrifices possible generalization ability to other unseen conditions during user interfaces.

To tackle the aforementioned limitations, we present a novel diffusion guidance named *Late-Constraint Diffusion Guidance (LCDG)*, which keeps the diffusion network unchanged and regularize its output to align with the external guidance. Fig. 1 illustrates the comparison between our *late-constraint* solution and *early-constraint* ones. Specifically, we train a lightweight condition adapter to capture the correlation between internal representations of diffusion models and external guidance. During sampling, we reformulate the estimated score of diffusion networks with the external control using corresponding trained adapter. Note that LCDG could serve as a plug-and-play tool for diffusion sampling of different backbones, and is compatible with their original sampling processes. Furthermore, we propose a timestep resampling strategy to ensure the stability of the proposed method, and introduce an early stopping technique to boost the sample quality meanwhile preserving the conditional guidance. Notably, the training of adapter is compute-efficient compared to early-constraint ones, which requires solely hours of training with small-scale self-collected data on a single 3090 GPU. Evaluation on COCO validation set [36] indicates that the proposed late-constraint solution obtains outperforming FID [19] and comparable CLIP score [46], compared to existing early-constraint ones [41, 66, 49]. Furthermore, experiments upon multiple applications with different diffusion backbones demonstrate the superiority of the proposed techniques. Our contribution could be summarized as:

1. We observe the limitations of existing *early-constraint* solutions, and present *Late-Constraint Diffusion Guidance*, which manages to align the output of the diffusion U-Net with the external guidance keeping the diffusion model unchanged.
2. We propose a lightweight and compute-efficient adapter to learn the correlation between the internal representations of the diffusion model and multiple external conditions.
3. Furthermore, we propose a timestep resampling strategy to stabilize the proposed method, and introduce an early stopping technique to boost the sample quality meanwhile preserving the effect of conditional guidance.
4. Evaluation upon public dataset demonstrates the promising performance of the proposed technique compared to existing early-constraint methods. Also, applications upon multiple conditions with both unconditional and text-to-image diffusion models illustrate the effectiveness and universal applicability of our method.

## 2 Related Work

**Image Synthesis and Translation.** Learning the high-dimensional data manifold of natural images is a great challenge for the topic of image synthesis, which have driven numerous efforts using different generative models, *e.g.*, GANs [28, 5, 29, 40, 27, 26], VAEs [57, 48], autoaggressive models [15, 9, 64, 33, 8, 34], and diffusion models [20, 21, 55, 43, 54, 3, 51, 12]. Furthermore, conditional

generative methods [25, 60, 44, 15, 64, 33, 51, 49] are also investigated, which utilize information in other domains to guide the synthesis process, *e.g.*, sketch, semantic map. Recently, text-to-image generative models [8, 16, 6, 49, 26] have come into prominence and emerged numerous inspiring applications, especially text-to-image diffusion models [49, 24, 52, 42, 17, 1, 31, 6, 16, 30, 37]. Such models have achieved significant performance for the community of conditional image synthesis.

**Controllable Image Synthesis for Diffusion Models.** Compared to Generative Adversarial Networks (GAN) [28, 5, 29, 40, 27, 26, 35, 65, 56, 67, 10, 50], diffusion models [20, 21, 55, 43, 54, 3, 17, 14, 49] have shown guaranteed training stability and superior generation ability across various benchmarks. Besides, text-to-image diffusion models [49, 17] reveal more controllability with guidance of text prompts. To provide more precise controls for diffusion models, several efforts [66, 41] have been further motivated. Known as *early-constraint* methods in this paper, they manage to provide intra-manipulations upon diffusion U-Net before output. However, such early-constraint solutions still reveal limitations, which may sacrifice much flexibility during user interfaces.

**Diffusion Guidance.** With solely modifications upon the sampling process, diffusion guidance reveal great flexibility and efficiency to manipulate diffusion sampling without retraining. Previous researches intend to enhance the sample quality of diffusion models using either noisy classifier [14] or the diffusion U-Net [22]. One related research with ours is SDG [37] attempting to introduce high-level guidance, *e.g.*, language and image, based on pre-trained CLIP [46] and DDPM [43]. But the potentials of discovering structural guidance from such aspect still remain to be investigated.

### 3 Approach

#### 3.1 Preliminaries

**Latent Diffusion Models.** We implement our method on both unconditional and text-to-image models of Stable Diffusion (SD) [49]. SD is implemented as a two-stage architecture. It first encodes the RGB image  $x_0$  into its corresponding latent representation  $z_0$  using a pre-trained VQ-GAN [15]. Then, it learns the reverse denoising process of a fixed Markov Chain of length  $T$  in the latent space. The optimization objective could be formulated as:

$$\mathcal{L} = \mathbb{E}_{z,c,\epsilon \sim \mathcal{N}(0,1),t} \left[ \|\epsilon - \epsilon_\theta(z_t, t, c)\|_2^2 \right], \quad (1)$$

where  $z_t = \sqrt{\bar{\alpha}_t}z_0 + \sqrt{1 - \bar{\alpha}_t}\epsilon$ ,  $\epsilon \sim \mathcal{N}(0, I)$ , representing the process of adding a  $t$ -step noise to  $z_0$ .  $\epsilon_\theta(z_t, t, c)$  denotes the estimated score. In the case of text-to-image generation,  $\epsilon_\theta(z_t, t, c)$  is conditioned on  $c$ , which denotes the text embeddings extracted by external text encoders [46, 11].

**Sampling.** During sampling of diffusion models, also known as the iterative denoising process, we start from a random Gaussian noise  $z_T$ . In text-to-image generation case, the sampling process is conditioned on the  $c$  extracted from the user-provided text prompts. Given  $t \in \{T, T - 1, \dots, 1, 0\}$ , the diffusion U-Net estimates the sampling score  $\epsilon_t$  and iteratively subtracts noises from the intermediate sample  $z_t$ , where we eventually obtains the clean sample  $z_0$ .

#### 3.2 Correlating by Reconstructing

Our goal is to manipulate diffusion sampling with external condition in a late-constraint manner. We first manage to discover the correlation between the output of diffusion U-Net and the external condition. Recently, diffusion models are proven to obtain well-differentiated internal representations, which highly correlate with semantic knowledge of the source images [2, 62]. We draw motivation from such solutions, and manage to learn the correlation towards more unexplored conditions.

**Condition Adapter.** Therefore, we propose Condition Adapter (CA), a lightweight CNN adapter to capture the correlation by learning to reconstruct the external conditions. Given an RGB image  $x_0 \in \mathbb{R}^{H \times W \times C}$ , we first encode it into the latent representation  $z_0$  using [15]. We add  $t$ -step noises to  $z_0$  according to  $q(z_t|z_0) := \mathcal{N}(z_t; \sqrt{\bar{\alpha}_t}z_0, (1 - \bar{\alpha}_t)I)$ , and obtains the noisy representation  $z_t$  with  $z_t = \sqrt{\bar{\alpha}_t}z_0 + \sqrt{1 - \bar{\alpha}_t}\epsilon$ ,  $\epsilon \sim \mathcal{N}(0, I)$ . Then, we extract a series of internal representations  $\{\mathcal{F}_i\}_{i=1}^N$  from different blocks  $\{1, 2, \dots, N\}$  in the diffusion U-Net passing  $z_t$  forward. Note that in the case of text-to-image generation [49], the forward process is conditioned on the text embeddings  $c$  extracted by text encoders [46, 11].  $\{\mathcal{F}_i\}_{i=1}^N$  are then aligned and integrated as  $\mathcal{F}$  by upsampling and concatenating them. Eventually, we train CA to reconstruct the external condition from the given  $\mathcal{F}$ .

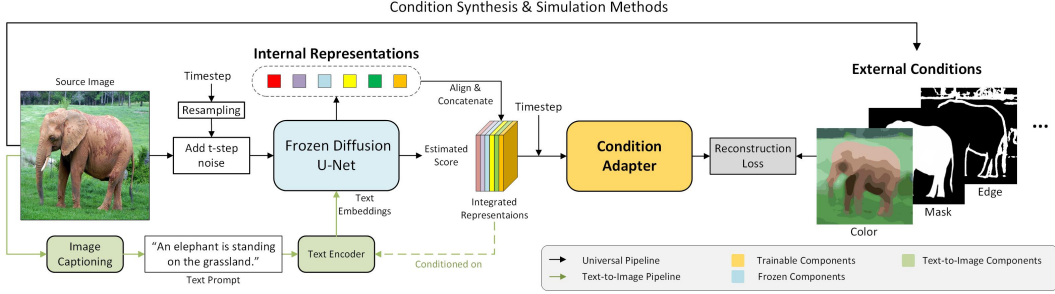


Figure 2: Illustration of the training pipeline of LCDG. Keeping the diffusion networks unchanged, our proposed LCDG requires to train a lightweight Condition Adapter (CA), to capture the correlation between the internal representations of diffusion models with external conditions.

In practice, it is natural to implement CA as CNN-based architecture to capture local structural information from the internal representations. Notably with a few stacks of convolution blocks, CA is able to learn the correlation. Each block is a two-branch design, which processes the input representations  $\mathcal{F}$  and timestep  $t$ , respectively. We follow the implementation in the U-Net of SD [43] using a sigmoid linear unit (SiLU) and a linear layer to formulate the timestep branch. The other branch is simply implemented with architecture of Conv-ReLU-BN.  $t$  is encoded into time embeddings and merged to the intermediate features in each block. CA learns to reconstruct the structural conditions supervised by  $\mathcal{C}_{ext}$ . The overall optimization objective could be formulated as:

$$\mathcal{L} = \|\mathbb{E}_\phi(\mathcal{F}, t) - \mathcal{C}_{ext}\|_2^2, \quad (2)$$

where  $\mathbb{E}_\phi$  denotes CA with  $\phi$  as its model weights. Note that the training of CA is compute-efficient and fast to implement, which only requires hours of training on a single 3090 GPU per condition. Also, the training of CA is dataset-free, which could be well implemented with small-scale self-collected data and automatically synthetic labels (Sec. 4).

**Timestep Resampling.** Timestep is an essential variable for diffusion models, which is highly associated with the magnitude of noise. During the training process of SD [49], the timestep  $t$  is randomly sampled from a uniform distribution  $U(0, T)$ . During sampling, the diffusion U-Net iteratively subtracts noise in the intermediate sample  $z_t$  with  $t$  starting from  $t = T$  to  $t = 0$ . As is known that the overall contents of diffusion models are determined at the beginning stage during sampling [41], which indicates that CA is expected to handle highly dynamic noisy samples  $z_t$  with different contents and levels of noises. To this end, we propose to resample the timestep  $t$  instead of sampling it from a uniform distribution  $U(0, T)$ . Given a uniform-sampled timestep as  $\hat{t}_{uni} = T - t$ ,  $t \in \{1, 2, \dots, T\}$ , the resampled timestep  $\hat{t}$  becomes:

$$\hat{t} = \left[1 - \left(\frac{t}{T}\right)^n\right] \times T, \quad (3)$$

where  $t \in \{1, 2, \dots, T\}$ .  $n$  is a hyperparameter that determines the magnitude of resampling. Compared to the uniform-sampled timestep  $\hat{t}_{uni}$ , the curve of  $\hat{t}$  with resampling is a convex function, where for each input  $t$ , the resampled timestep obtains a greater value than the original one.

### 3.3 Structure-Aware Diffusion Sampling

During inference, we manipulate the diffusion sampling with the external guidance and corresponding adapter. We demonstrate some applications of practical usage with a series of structural guidance, including edge, sketch, color stroke, palette, and mask, denoting the manipulated sampling process as *Structure-Aware Diffusion Sampling*. Fig. 3 shows the visualizations of text-to-image diffusion sampling and the guided one. One could see that LCDG aligns the intermediate samples with the external guidance and stabilizes corresponding conditions with the learned correlation. For one manipulated sampling step  $t$ , we obtain the internal representations of  $z_t$  from the diffusion U-Net, and reconstruct its corresponding condition  $\mathcal{C}$ . Then, we obtain the difference map between  $\mathcal{C}$  and the external condition  $\mathcal{C}_{ext}$  by calculating the latent distance between them, written as  $\Delta\mathcal{C} = \text{dist}(\mathcal{C}, \mathcal{C}_{ext})$ . The condition score  $\epsilon_{str}$  correlated to the structural guidance is then computed in forms of gradients with respect to  $z_t$ . Furthermore, we normalize  $\epsilon_{str}$  with a controlling scale  $\beta$ ,

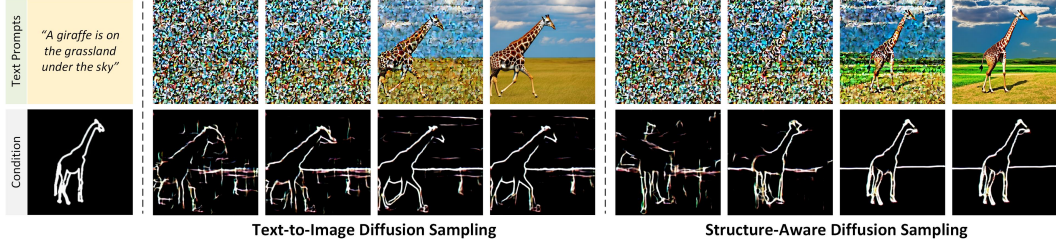


Figure 3: Visualizations of the intermediate samples and corresponding conditions under text-to-image diffusion sampling (left) and structure-aware diffusion sampling (right).

eventually reformulating the estimated score  $\epsilon_t$  of diffusion U-Net as:

$$\underbrace{\nabla_{z_t} \log p(z_t | c, \mathcal{C}_{ext})}_{\text{Reformulated Score}} = \underbrace{\nabla_{z_t} \log p(z_t | c)}_{\text{Estimated Score}} + \underbrace{\beta \nabla_{z_t} \log p(\Delta \mathcal{C} | z_t)}_{\text{Condition Score}}, \quad (4)$$

where the condition score could be obtained by corresponding CA. For the text-to-image generation scenario, the sampling process is conditioned on the text embeddings  $c$ . In brief, we summarize the sampling score using LCDG as  $\hat{\epsilon}_t = \epsilon_t + \beta \epsilon_{str}$ .

**Truncation Conditioned Sampling.** Motivated by the effectiveness of early stopping strategy [38] upon diffusion models, we manage to further explore its possible benefits for controllable image synthesis. Therefore, we propose Truncation Conditioned Sampling (TCS) strategy to boost the sample quality meanwhile preserving the guidance of external conditions. We discover that manipulating parts of the sampling process instead of the whole one obtains synthesized image in better quality, meanwhile accelerating the sampling process (Sec. 4.4). Specifically, we assign a truncation threshold  $T_{trunc} \in \{T, T-1, \dots, 1\}$ , and solely manipulate the steps in  $\{T, T-1, \dots, T_{trunc}\}$  during sampling. In a nutshell, the overall process of LCDG could be summarized as follows:

---

#### Algorithm 1 Structure-Aware Diffusion Sampling

---

**Input:** Target condition  $\mathcal{C}_{ext}$ , frozen diffusion U-net  $(\mu_\theta, \sigma_\theta)$ , controlling scale  $\beta$ , truncation threshold of TCS  $T_{trunc}$   
**Output:** result  $z_0$   
 $z_T \leftarrow N(0, \mathbf{I})$   
 $\mu, \Sigma \leftarrow \mu_\theta, \sigma_\theta^2 \mathbf{I}$   
**for**  $t = T, \dots, T_{trunc}$  **do** ▷ Sample from the conditional distribution  
 $z_{t-1} \leftarrow \mathcal{N}(\mu + \beta \Sigma g_{str}, \sigma_\theta^2 \mathbf{I})$   
**end for**  
**for**  $t' = T_{trunc} - 1, \dots, 1, 0$  **do** ▷ Sample from the original distribution  
 $z_{t'-1} \leftarrow \mathcal{N}(\mu, \sigma_\theta^2 \mathbf{I})$   
**end for**  
**return**  $z_0$

---

Here,  $g_{str}$  represents the shifted mean correlated to external conditions, written as  $\nabla_{z_t} \log p(\Delta \mathcal{C} | z_t)$ . Note that the process is conditioned on extracted text embeddings  $c$  in the case of text-to-image generation. It is proven that the conditional distribution could be approximated by a Gaussian distribution with a shifted mean in the case of class-conditional image synthesis [14]. LCDG embodies as a broader case of structural conditions that using LCDG essentially samples from the conditional distribution associated with the structural guidance. The aforementioned algorithm also illustrates the compatibility of LCDG with the original sampling process, which provides more flexibility and controllability for users to customize their manipulations.

## 4 Experiments

### 4.1 Experimental Setup

**Implementation Details.** LCDG is compute-efficient and fast to implement. We notice that current early-constraint methods [41, 66] still rely on annotated datasets in million scales for training,

Table 1: Quantitative comparison on COCO 2017 validation set [36], compared to SD\* [49], ControlNet [66], and T2I-Adapter [41]. The **best** results under each setting are highlighted. Note that we use HED edge [61] for evaluation of edge condition. SD\*: Stable Diffusion [49] using SDEdit [39]. T2I-Adapter\*: Reproduced results.

Method	Condition	FID $\downarrow$	CLIP Score $\uparrow$
SD [49]	text	27.99	0.2673
ControlNet [66]	text + edge	28.09	0.2525
T2I-Adapter* [41]	text + edge	21.72	<b>0.2597</b>
<b>Ours</b>	text + edge	<b>21.02</b>	0.2590
SD* [49]	text + stroke	32.93	0.2257
T2I-Adapter [41]	text + stroke	30.84	0.2587
<b>Ours</b>	text + stroke	<b>20.27</b>	<b>0.2589</b>
SD* [49]	text + palette	71.16	0.2138
T2I-Adapter [41]	text + palette	26.54	<b>0.2613</b>
<b>Ours</b>	text + palette	<b>20.61</b>	0.2580
<b>Ours</b>	text + mask	<b>20.94</b>	<b>0.2617</b>

*e.g.*, COCO. In reverse, LCDG works as a dataset-free solution, which could perform well with training of small-scale self-collected data and synthetic labels. For training, we randomly collect 10,000 images from the internet and automatically annotate their corresponding captions using a pre-trained image captioning model [23]. We summarize the implementations of LCDG on three main domains of structural conditions: *edge*, *color*, and *mask*. Note that each domain of the implemented conditions shares the same model during inference. *Edge condition* includes Canny edge [7], HED-like edge [61], and user sketch. We use a HED-like edge detector [18] together with some data augmentation strategies to simulate the supervision signal, which includes random thresholds, random warping, random dilation and corrosion. *Color condition* consists of color stroke and image palette. We refer to the human-stroke simulation algorithm in [39] with augmentation of varying the k-means center, and simulate the image palette by resizing source images using the nearest interpolation. *Mask condition* contains binary masks in different grained levels. We demonstrate some instances in Fig. 5 that coarse-grained user scribbles intend to guide the abstract position in the generated contents, and fine-grained segmentation masks manage to locate the precise shape and position of the salient objects. To simulate the supervision labels, we use a pre-trained saliency detection model [45] to detect masks from source images.

**Evaluation Setting.** For evaluation, we compare LCDG to state-of-the-art conditional text-to-image synthesis methods as well as early-constraint solutions, including SD\* [49] (SD using SDEdit [39], for comparison of stroke condition), ControlNet [66], and T2I-Adapter [41]. Text-to-image SD [49] is also evaluated for reference. Besides, we implement cross evaluations to measure the performance of early-constraint solutions upon other unseen conditions. Evaluations are implemented on COCO 2017 validation set [36] using the official annotated captions. We use FID score [19] and CLIP score [46] (using ViT/L-14 model) as evaluation metrics, and SD [49] with version of 1.4 as our base model during evaluation. Note that we could not reproduce the result of [41] as good as their reported one, and provide our reproduced one in Tab. 1. We would open-source our evaluation code and provide evaluation details in our supplementary materials.

**Demonstrated Applications.** LCDG provides a paradigm to introduce external conditions into diffusion sampling, which should be compatible with different kinds of diffusion backbones. Out of demonstration, we show some applications of LCDG upon multiple structural conditions, and both unconditional and text-to-image diffusion models [49]. For unconditional generation setting, we demonstrate some conditional generation tasks in the face domain with SD [49] trained on CelebA-HQ [27]. For text-to-image generation setting, we use text-to-image SD [49] with version of 2.1 for applications. Note that we implement *edge* and *color* conditions on unconditional applications, and all three domains on text-to-image ones.

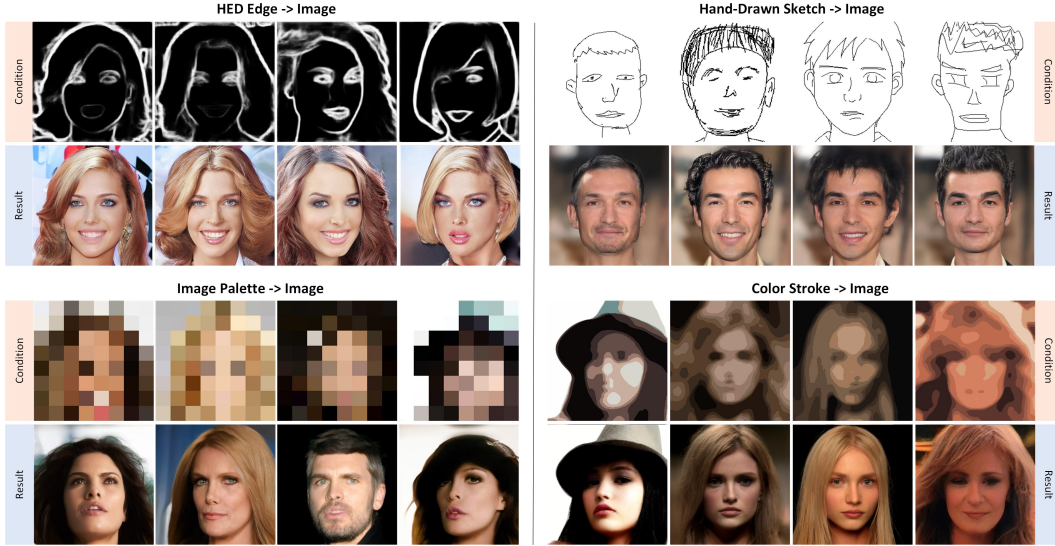


Figure 4: Conditional image synthesis results of LCDG, implemented with unconditional SD [49] trained CelebA-HQ [27]. Each row of the results share the same model during inference. For hand-drawn sketches, we choose the proposed sketch set in [63] for evaluation.

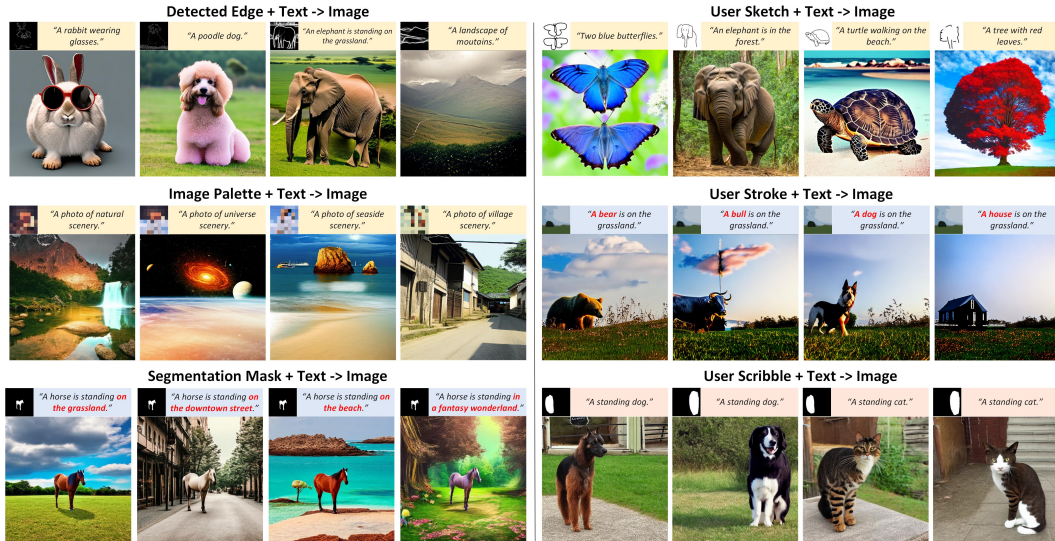


Figure 5: Conditional text-to-image synthesis results of LCDG, implemented with text-to-image SD [49]. Note that each row of the cases share the same model during inference.

## 4.2 Evaluation

Tab. 1 reports the quantitative results of LCDG compared to state-of-the-art competitors [59, 66, 41, 49] under different conditions. Our method outperforms others in FID [19] under all settings, indicating the promising sample quality of LCDG. Note that all compared methods obtain lower CLIP scores than text-to-image SD [49] does. But the proposed LCDG obtains the least deterioration in most cases and comparable performance. For the cross evaluation for early-constraint solutions [49, 41], one could see that such methods fail the generalization process, thereby obtaining obvious performance drop in such conditions compared to their implemented ones.

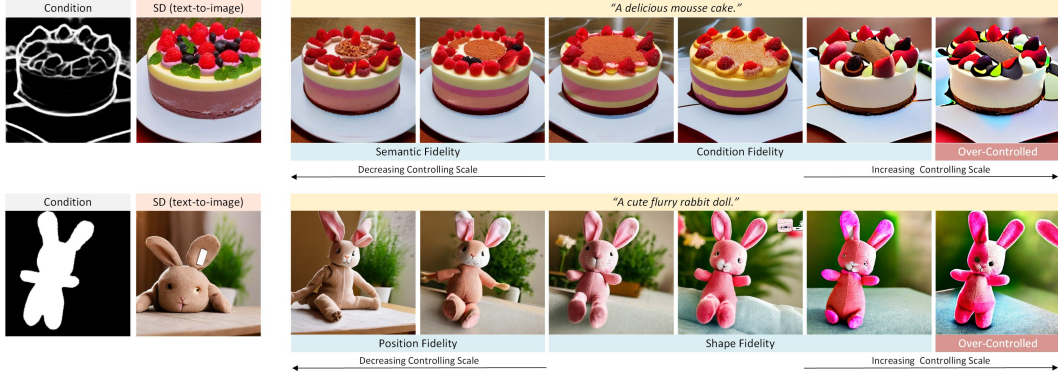


Figure 6: Qualitative results for ablation studies of controlling scale.



Figure 7: Qualitative results for ablation studies of truncation threshold of TCS.

### 4.3 Applications

Fig. 4 reports some applications using LCDG for conditional generation tasks in the face domain. And Fig. 5 shows some conditional text-to-image applications using LCDG. As is shown in Fig. 4 and Fig. 5, LCDG is capable of supporting both synthesized (left) and user-provided conditions (right). One can see that using LCDG allows users to confirm their desired overall structure of the generated results in the first place, then let diffusion models sample from the original distribution to produce realistic details in the remaining steps. By using different text prompts, users could further enrich the semantic information of the generated contents. Notably, each separated row of showcases shares the same model weights, *e.g.*, color stroke and image palette, indicating the plausible generalization ability of LCDG to similar conditions in near domains without retraining. In Fig 6 and Fig. 7, applications for controllable image synthesis demonstrate the flexibility of LCDG, and the computational advantage without retraining over early-constraint solutions [66, 41, 60].

### 4.4 Ablation Study

**Controlling Scale.** The controlling scale is a vital component of LCDG, which determines the weight of the condition score at each guided sampling step. Fig. 8 (a) reports the curve of FID [19] for the ablation study and Fig. 6 shows corresponding qualitative results. By varying the controlling scale, LCDG provides plausible controllability for users to focus on different aspects of the guidance. One could see that the sampling process is manipulated leniently and focus more on semantic fidelity. As the controlling scale increases, samples are more strictly controlled concentrating more on the condition fidelity. Notably, the samples would be severely deteriorated once over-controlled.

**Truncation Threshold of TCS.** The truncation threshold of the TCS strategy determines the number of manipulated steps during diffusion sampling. Also, it demonstrates the controllability of LCDG from another perspective. Fig. 8 (b) reports the FID scores [19] and Fig. 7 shows corresponding qualitative results. The smaller the truncation threshold is, the more steps are manipulated. LCDG

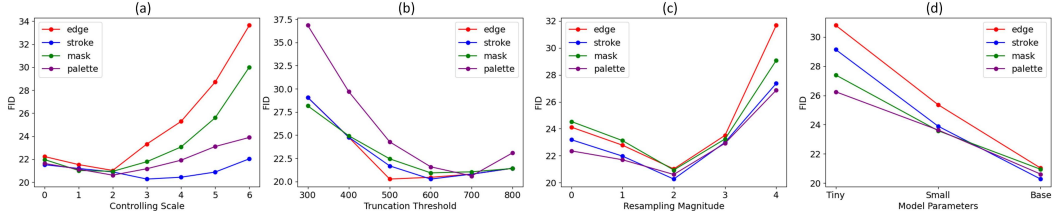


Figure 8: Curves of FID scores for ablation studies of (a) controlling scale, (b) truncation threshold, (c) timestep resampling magnitude, and (d) model parameters of CA.



Figure 9: Qualitative results for the ablation studies of timestep resampling magnitude.

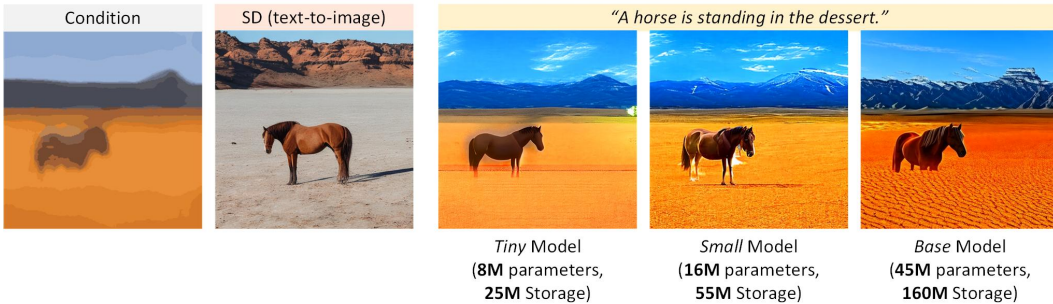


Figure 10: Qualitative results for the ablation studies of model parameters of CA.

is able to provide effective regularization with solely a few steps manipulated. The samples further follow the exact color and boundaries as the threshold increases. Without TCS, the details of samples would be severely deteriorated or reveal checkerboard artifacts. Also, the sampling speed (22.01s) would obviously slower than the one using TCS (11.94s, both tested on a single 3090 GPU).

**Magnitude of Timestep Resampling.** The timestep resampling strategy ensures the stability of LCDG while processing the highly dynamic noisy inputs during sampling. Fig. 8 (c) and Fig. 9 report the ablation study both quantitatively and qualitatively. On one hand, we expect such augmentation strategy could benefit the training of CA sufficiently, where the FID scores and details of the samples gradually improve until the magnitude reaches the optimal one ( $n = 2$ ). As  $n$  keeps increasing greater, the training data becomes over-noised. LCDG fails the manipulation upon diffusion sampling, and produces inaccurately controlled results with less details.

**Model Parameters.** In addition to a series of hyperparameters of LCDG, we also ablate the minimum model parameters of CA and the performance lower bound of LCDG. Fig. 8 (d) and Fig. 10 report the ablated results. We decrease the model parameters by removing several layers in CA and compress the network channels. It is worth noting that LCDG is still capable of constraining the sampling process even with model parameter of **8M** (*tiny* model), which proves the effectiveness of the design of LCDG once again. However, since CA could solely learn simple relationship between the internal representations and structural characteristics, the manipulated diffusion sampling tend to produce controlled results with less photorealistic details.

## 5 Conclusions and Discussions

We present an innovative solution for controllable image synthesis, called *Late-Constrained Diffusion Guidance (LCDG)*, to manipulate diffusion sampling with external guidance meanwhile preserving the diffusion networks unchanged. Boosted by strategies like timestep resampling and truncation conditioned sampling, LCDG reveals promising performance for controllable image synthesis, and great generalization ability and flexibility over existing early-constraint methods. However, LCDG still suffers from some limitations that gradient-based methods [14, 22] share, which would increase the sampling speed with additional forwarding processes of the diffusion U-Net. In our supplementary materials, we would illustrate more details and present more applications of the proposed LCDG.

## References

- [1] Omri Avrahami, Dani Lischinski, and Ohad Fried. Blended diffusion for text-driven editing of natural images. In *CVPR*, pages 18208–18218, 2022.
- [2] Dmitry Baranchuk, Ivan Rubachev, Andrey Voynov, Valentin Khrukov, and Artem Babenko. Label-efficient semantic segmentation with diffusion models. *arXiv preprint arXiv:2112.03126*, 2021.
- [3] Andreas Blattmann, Robin Rombach, Kaan Oktay, Jonas Müller, and Björn Ommer. Retrieval-augmented diffusion models. *NeurIPS*, 35:15309–15324, 2022.
- [4] Daniel Bolya, Cheng-Yang Fu, Xiaoliang Dai, Peizhao Zhang, Christoph Feichtenhofer, and Judy Hoffman. Token merging: Your vit but faster. *arXiv preprint arXiv:2210.09461*, 2022.
- [5] Andrew Brock, Jeff Donahue, and Karen Simonyan. Large scale gan training for high fidelity natural image synthesis. *arXiv preprint arXiv:1809.11096*, 2018.
- [6] Tim Brooks, Aleksander Holynski, and Alexei A Efros. Instructpix2pix: Learning to follow image editing instructions. *arXiv preprint arXiv:2211.09800*, 2022.
- [7] John Canny. A computational approach to edge detection. *TPAMI*, (6):679–698, 1986.
- [8] Huiwen Chang, Han Zhang, Jarred Barber, AJ Maschinot, Jose Lezama, Lu Jiang, Ming-Hsuan Yang, Kevin Murphy, William T Freeman, Michael Rubinstein, et al. Muse: Text-to-image generation via masked generative transformers. *arXiv preprint arXiv:2301.00704*, 2023.
- [9] Huiwen Chang, Han Zhang, Lu Jiang, Ce Liu, and William T Freeman. Maskgit: Masked generative image transformer. In *CVPR*, pages 11315–11325, 2022.
- [10] Jun Cheng, Fuxiang Wu, Yanling Tian, Lei Wang, and Dapeng Tao. Rifegan: Rich feature generation for text-to-image synthesis from prior knowledge. In *CVPR*, pages 10911–10920, 2020.
- [11] Mehdi Cherti, Romain Beaumont, Ross Wightman, Mitchell Wortsman, Gabriel Ilharco, Cade Gordon, Christoph Schuhmann, Ludwig Schmidt, and Jenia Jitsev. Reproducible scaling laws for contrastive language-image learning. *arXiv preprint arXiv:2212.07143*, 2022.
- [12] Jooyoung Choi, Sungwon Kim, Yonghyun Jeong, Youngjune Gwon, and Sungroh Yoon. Ilvr: Conditioning method for denoising diffusion probabilistic models. *arXiv preprint arXiv:2108.02938*, 2021.
- [13] Jia Deng, Wei Dong, Richard Socher, Li-Jia Li, Kai Li, and Li Fei-Fei. Imagenet: A large-scale hierarchical image database. In *2009 IEEE conference on computer vision and pattern recognition*, pages 248–255. Ieee, 2009.
- [14] Prafulla Dhariwal and Alexander Nichol. Diffusion models beat gans on image synthesis. *NeurIPS*, 34:8780–8794, 2021.
- [15] Patrick Esser, Robin Rombach, and Bjorn Ommer. Taming transformers for high-resolution image synthesis. In *CVPR*, pages 12873–12883, 2021.
- [16] Oran Gafni, Adam Polyak, Oron Ashual, Shelly Sheynin, Devi Parikh, and Yaniv Taigman. Make-a-scene: Scene-based text-to-image generation with human priors. In *Computer Vision—ECCV 2022: 17th European Conference, Tel Aviv, Israel, October 23–27, 2022, Proceedings, Part XV*, pages 89–106. Springer, 2022.
- [17] Shuyang Gu, Dong Chen, Jianmin Bao, Fang Wen, Bo Zhang, Dongdong Chen, Lu Yuan, and Baining Guo. Vector quantized diffusion model for text-to-image synthesis. In *CVPR*, pages 10696–10706, 2022.
- [18] Jianzhong He, Shiliang Zhang, Ming Yang, Yanhu Shan, and Tiejun Huang. Bdcn: Bi-directional cascade network for perceptual edge detection. *TPAMI*, 44(1):100–113, 2020.
- [19] Martin Heusel, Hubert Ramsauer, Thomas Unterthiner, Bernhard Nessler, and Sepp Hochreiter. Gans trained by a two time-scale update rule converge to a local nash equilibrium. In I. Guyon, U. Von Luxburg, S. Bengio, H. Wallach, R. Fergus, S. Vishwanathan, and R. Garnett, editors, *NeurIPS*, volume 30. Curran Associates, Inc., 2017.

- [20] Jonathan Ho, Ajay Jain, and Pieter Abbeel. Denoising diffusion probabilistic models. *NeurIPS*, 33:6840–6851, 2020.
- [21] Jonathan Ho, Chitwan Saharia, William Chan, David J Fleet, Mohammad Norouzi, and Tim Salimans. Cascaded diffusion models for high fidelity image generation. *J. Mach. Learn. Res.*, 23(47):1–33, 2022.
- [22] Jonathan Ho and Tim Salimans. Classifier-free diffusion guidance. *arXiv preprint arXiv:2207.12598*, 2022.
- [23] Jia Cheng Hu, Roberto Cavicchioli, and Alessandro Capotondi. Expansionnet v2: Block static expansion in fast end to end training for image captioning. *arXiv preprint arXiv:2208.06551*, 2022.
- [24] Lianghua Huang, Di Chen, Yu Liu, Yujun Shen, Deli Zhao, and Jingren Zhou. Composer: Creative and controllable image synthesis with composable conditions. *arXiv preprint arXiv:2302.09778*, 2023.
- [25] Phillip Isola, Jun-Yan Zhu, Tinghui Zhou, and Alexei A Efros. Image-to-image translation with conditional adversarial networks. In *CVPR*, pages 1125–1134, 2017.
- [26] Minguk Kang, Jun-Yan Zhu, Richard Zhang, Jaesik Park, Eli Shechtman, Sylvain Paris, and Taesung Park. Scaling up gans for text-to-image synthesis. *arXiv preprint arXiv:2303.05511*, 2023.
- [27] Tero Karras, Timo Aila, Samuli Laine, and Jaakko Lehtinen. Progressive growing of gans for improved quality, stability, and variation. *arXiv preprint arXiv:1710.10196*, 2017.
- [28] Tero Karras, Samuli Laine, and Timo Aila. A style-based generator architecture for generative adversarial networks. In *CVPR*, pages 4401–4410, 2019.
- [29] Tero Karras, Samuli Laine, Miika Aittala, Janne Hellsten, Jaakko Lehtinen, and Timo Aila. Analyzing and improving the image quality of stylegan. In *CVPR*, pages 8110–8119, 2020.
- [30] Bahjat Kawar, Shiran Zada, Oran Lang, Omer Tov, Huiwen Chang, Tali Dekel, Inbar Mosseri, and Michal Irani. Imagic: Text-based real image editing with diffusion models. *arXiv preprint arXiv:2210.09276*, 2022.
- [31] Gwanghyun Kim, Taesung Kwon, and Jong Chul Ye. Diffusionclip: Text-guided diffusion models for robust image manipulation. In *CVPR*, pages 2426–2435, 2022.
- [32] Diederik P. Kingma and Jimmy Ba. Adam: A method for stochastic optimization. In Yoshua Bengio and Yann LeCun, editors, *3rd International Conference on Learning Representations, ICLR 2015, San Diego, CA, USA, May 7-9, 2015, Conference Track Proceedings*, 2015.
- [33] Doyup Lee, Chiheon Kim, Saehoon Kim, Minsu Cho, and Wook-Shin Han. Autoregressive image generation using residual quantization. In *CVPR*, pages 11523–11532, 2022.
- [34] Tianhong Li, Huiwen Chang, Shlok Kumar Mishra, Han Zhang, Dina Katabi, and Dilip Krishnan. Mage: Masked generative encoder to unify representation learning and image synthesis. *arXiv preprint arXiv:2211.09117*, 2022.
- [35] Jiadong Liang, Wenjie Pei, and Feng Lu. Cpgan: Content-parsing generative adversarial networks for text-to-image synthesis. In *ECCV*, pages 491–508. Springer, 2020.
- [36] Tsung-Yi Lin, Michael Maire, Serge Belongie, James Hays, Pietro Perona, Deva Ramanan, Piotr Dollár, and C Lawrence Zitnick. Microsoft coco: Common objects in context. In *ECCV*, pages 740–755. Springer, 2014.
- [37] Xihui Liu, Dong Huk Park, Samaneh Azadi, Gong Zhang, Arman Chopikyan, Yuxiao Hu, Humphrey Shi, Anna Rohrbach, and Trevor Darrell. More control for free! image synthesis with semantic diffusion guidance. In *WACV*, pages 289–299, 2023.
- [38] Zhaoyang Lyu, Xudong Xu, Ceyuan Yang, Dahua Lin, and Bo Dai. Accelerating diffusion models via early stop of the diffusion process. *arXiv preprint arXiv:2205.12524*, 2022.
- [39] Chenlin Meng, Yang Song, Jiaming Song, Jiajun Wu, Jun-Yan Zhu, and Stefano Ermon. Sdedit: Image synthesis and editing with stochastic differential equations. *arXiv preprint arXiv:2108.01073*, 2021.
- [40] Takeru Miyato, Toshiki Kataoka, Masanori Koyama, and Yuichi Yoshida. Spectral normalization for generative adversarial networks. *arXiv preprint arXiv:1802.05957*, 2018.
- [41] Chong Mou, Xintao Wang, Liangbin Xie, Jian Zhang, Zhongang Qi, Ying Shan, and Xiaohu Qie. T2i-adapter: Learning adapters to dig out more controllable ability for text-to-image diffusion models. *arXiv preprint arXiv:2302.08453*, 2023.
- [42] Alex Nichol, Prafulla Dhariwal, Aditya Ramesh, Pranav Shyam, Pamela Mishkin, Bob McGrew, Ilya Sutskever, and Mark Chen. Glide: Towards photorealistic image generation and editing with text-guided diffusion models. *arXiv preprint arXiv:2112.10741*, 2021.
- [43] Alexander Quinn Nichol and Prafulla Dhariwal. Improved denoising diffusion probabilistic models. In *ICML*, pages 8162–8171. PMLR, 2021.

- [44] Taesung Park, Ming-Yu Liu, Ting-Chun Wang, and Jun-Yan Zhu. Semantic image synthesis with spatially-adaptive normalization. In *CVPR*, pages 2337–2346, 2019.
- [45] Xuebin Qin, Zichen Zhang, Chenyang Huang, Masood Dehghan, Osmar R Zaiane, and Martin Jagersand. U2-net: Going deeper with nested u-structure for salient object detection. *Pattern Recognit.*, 106:107404, 2020.
- [46] Alec Radford, Jong Wook Kim, Chris Hallacy, Aditya Ramesh, Gabriel Goh, Sandhini Agarwal, Girish Sastry, Amanda Askell, Pamela Mishkin, Jack Clark, et al. Learning transferable visual models from natural language supervision. In *ICML*, pages 8748–8763. PMLR, 2021.
- [47] Colin Raffel, Noam Shazeer, Adam Roberts, Katherine Lee, Sharan Narang, Michael Matena, Yanqi Zhou, Wei Li, and Peter J Liu. Exploring the limits of transfer learning with a unified text-to-text transformer. *The Journal of Machine Learning Research*, 21(1):5485–5551, 2020.
- [48] Ali Razavi, Aaron Van den Oord, and Oriol Vinyals. Generating diverse high-fidelity images with vq-vae-2. *NeurIPS*, 32, 2019.
- [49] Robin Rombach, Andreas Blattmann, Dominik Lorenz, Patrick Esser, and Björn Ommer. High-resolution image synthesis with latent diffusion models. In *CVPR*, pages 10684–10695, 2022.
- [50] Shulan Ruan, Yong Zhang, Kun Zhang, Yanbo Fan, Fan Tang, Qi Liu, and Enhong Chen. Dae-gan: Dynamic aspect-aware gan for text-to-image synthesis. In *ICCV*, pages 13960–13969, 2021.
- [51] Chitwan Saharia, William Chan, Huiwen Chang, Chris Lee, Jonathan Ho, Tim Salimans, David Fleet, and Mohammad Norouzi. Palette: Image-to-image diffusion models. In *SIGGRAPH*, pages 1–10, 2022.
- [52] Chitwan Saharia, William Chan, Saurabh Saxena, Lala Li, Jay Whang, Emily L Denton, Kamyar Ghasemipour, Raphael Gontijo Lopes, Burcu Karagol Ayan, Tim Salimans, et al. Photorealistic text-to-image diffusion models with deep language understanding. *NeurIPS*, 35:36479–36494, 2022.
- [53] Patsorn Sangkloy, Nathan Burnell, Cusuh Ham, and James Hays. The sketchy database: learning to retrieve badly drawn bunnies. *ACM Trans. Graph.*, 35(4):1–12, 2016.
- [54] Jiaming Song, Chenlin Meng, and Stefano Ermon. Denoising diffusion implicit models. *arXiv preprint arXiv:2010.02502*, 2020.
- [55] Yang Song, Jascha Sohl-Dickstein, Diederik P Kingma, Abhishek Kumar, Stefano Ermon, and Ben Poole. Score-based generative modeling through stochastic differential equations. *arXiv preprint arXiv:2011.13456*, 2020.
- [56] Ming Tao, Hao Tang, Songsong Wu, Nicu Sebe, Xiao-Yuan Jing, Fei Wu, and Bingkun Bao. Df-gan: Deep fusion generative adversarial networks for text-to-image synthesis. *arXiv preprint arXiv:2008.05865*, 2020.
- [57] Aaron Van Den Oord, Oriol Vinyals, et al. Neural discrete representation learning. *NeurIPS*, 30, 2017.
- [58] Ashish Vaswani, Noam Shazeer, Niki Parmar, Jakob Uszkoreit, Llion Jones, Aidan N Gomez, Łukasz Kaiser, and Illia Polosukhin. Attention is all you need. In I. Guyon, U. Von Luxburg, S. Bengio, H. Wallach, R. Fergus, S. Vishwanathan, and R. Garnett, editors, *Advances in Neural Information Processing Systems*, volume 30. Curran Associates, Inc., 2017.
- [59] Tengfei Wang, Ting Zhang, Bo Zhang, Hao Ouyang, Dong Chen, Qifeng Chen, and Fang Wen. Pretraining is all you need for image-to-image translation. *arXiv preprint arXiv:2205.12952*, 2022.
- [60] Ting-Chun Wang, Ming-Yu Liu, Jun-Yan Zhu, Andrew Tao, Jan Kautz, and Bryan Catanzaro. High-resolution image synthesis and semantic manipulation with conditional gans. In *CVPR*, pages 8798–8807, 2018.
- [61] Saining Xie and Zhuowen Tu. Holistically-nested edge detection. In *ICCV*, pages 1395–1403, 2015.
- [62] Jiarui Xu, Sifei Liu, Arash Vahdat, Wonmin Byeon, Xiaolong Wang, and Shalini De Mello. Open-vocabulary panoptic segmentation with text-to-image diffusion models. *arXiv preprint arXiv:2303.04803*, 2023.
- [63] Shuai Yang, Zhangyang Wang, Jiaying Liu, and Zongming Guo. Deep plastic surgery: Robust and controllable image editing with human-drawn sketches. In *ECCV*, pages 601–617. Springer, 2020.
- [64] Jiahui Yu, Yuanzhong Xu, Jing Yu Koh, Thang Luong, Gunjan Baid, Zirui Wang, Vijay Vasudevan, Alexander Ku, Yinfei Yang, Burcu Karagol Ayan, et al. Scaling autoregressive models for content-rich text-to-image generation. *arXiv preprint arXiv:2206.10789*, 2022.
- [65] Han Zhang, Jing Yu Koh, Jason Baldridge, Honglak Lee, and Yinfei Yang. Cross-modal contrastive learning for text-to-image generation. In *CVPR*, pages 833–842, 2021.
- [66] Lvmin Zhang and Maneesh Agrawala. Adding conditional control to text-to-image diffusion models. *arXiv preprint arXiv:2302.05543*, 2023.
- [67] Zhenxing Zhang and Lambert Schomaker. Dtgan: Dual attention generative adversarial networks for text-to-image generation. In *IJCNN*, pages 1–8. IEEE, 2021.

## A Overview

We formulate our supplementary materials as follows. Sec. B provides a detailed mathematical Illustration of our proposed Late-Constraint Diffusion Guidance (LCDG). Sec. C provide the details of network architecture of the proposed Condition Adapter (CA), pipelines for data preparation, training implementations, and evaluation settings. We discuss some limitations of LCDG in Sec. D, and propose possible solutions to address them. In Sec. E, we further ablate the domains of training data and minimum training iteration of CA. In Sec. F, we report more qualitative results with both unconditional and text-to-image diffusion models, and comparison to state-of-the-art conditional image synthesis methods [49, 41, 66].

## B Mathematical Illustration

We start with the text-to-image conditional denoising process  $p(z_t|z_{t+1}, c)$ , where  $c$  represents the extracted text embeddings using a pre-trained CLIP [46]. Given the external control signal as  $\mathcal{C}_{ext}$ , it suffices to sample each noise subtracting process according to:

$$p_\theta(z_{t-1}|z_t, c, \mathcal{C}_{ext}) = \alpha p_\theta(z_{t-1}|z_t, c) p_\psi(\mathcal{C}_{ext}|z_{t-1}), \quad (5)$$

where  $\alpha$  is a normalization weight to maintain the conditional score to have the same magnitude as other terms in the sampling score, written as  $\frac{\|z_t - z_{t-1}\|_2^2}{\|\nabla_{z_t} \mathbf{dist}(\mathcal{C}, \mathcal{C}_{ext})\|_2^2}$ .  $\theta$  is the diffusion model and  $\psi$  represents the proposed Condition Adapter (CA). Given an RGB image  $x_0$ , we denote its corresponding latent representation as  $z$  in the following derivation. We refer to the derivation of [14] and review the one of ours. Starting from that the pre-trained diffusion model [49] which estimates the previous timestep  $z_{t-1}$  from  $z_t$  using a Gaussian distribution:

$$\begin{aligned} p_\theta(z_{t-1}|z_t, c) &= \mathcal{N}(\mu, \Sigma), \\ \log p_\theta(z_{t-1}|z_t, c) &= -\frac{1}{2}(z_{t-1} - \mu)^T \Sigma^{-1}(z_{t-1} - \mu). \end{aligned} \quad (6)$$

Similarly, given the limit of the diffusion steps is infinite where  $\|\Sigma\| \rightarrow 0$ , we could assume that  $\log_\psi(\mathcal{C}|z_t)$  is low-curvatures compared to  $\Sigma^{-1}$ . One different thing of LCDG from [14] is that we need to consider introducing the external condition  $\mathcal{C}_{ext}$  into this derivation process. To correlate the intermediate samples  $z_{t-1}$  with  $\mathcal{C}_{ext}$ , we observe the difference map  $\Delta\mathcal{C} = \mathbf{dist}(\mathcal{C} - \mathcal{C}_{ext})$ , where  $\mathbf{dist}()$  denotes L2 norm. Therefore, we could approximate  $\log p_\psi(\Delta\mathcal{C}|z_{t-1})$  using a Taylor expansion around  $z_{t-1} = \mu$  as:

$$\begin{aligned} \log p_\psi(\Delta\mathcal{C}|z_{t-1}) &\approx \log p_\psi(\Delta\mathcal{C}|z_{t-1})|_{z_{t-1}=\mu} + (z_{t-1} - \mu) \nabla_{z_{t-1}} \log p_\psi(\Delta\mathcal{C}|z_{t-1})|_{z_{t-1}=\mu}, \\ &= (z_{t-1} - \mu) g_{str}, \end{aligned} \quad (7)$$

where  $g_{str} = \nabla_{z_{t-1}} \log p_\psi(\Delta\mathcal{C}|z_{t-1})|_{z_{t-1}=\mu}$ , corresponding to the  $g_{str}$  in Alg. 1. By submitting Eqn. 6 and Eqn. 7 into Eqn. 5, we have:

$$\begin{aligned} \log [p_\theta(z_{t-1}|z_t) p_\psi(\Delta\mathcal{C}|z_{t-1})] &\approx -\frac{1}{2}(z_{t-1} - \mu)^T \Sigma^{-1}(z_{t-1} - \mu) + (z_{t-1} - \mu) g_{str} \\ &= -\frac{1}{2}(z_{t-1} - \mu - \Sigma g_{str})^T \Sigma^{-1}(z_{t-1} - \mu - \Sigma g_{str}) + \frac{1}{2} g_{str}^T \Sigma g_{str} \\ &= -\frac{1}{2}(z_{t-1} - \mu - \Sigma g_{str})^T \Sigma^{-1}(z_{t-1} - \mu - \Sigma g_{str}) \\ &= \log p_\theta(z), \end{aligned} \quad (8)$$

where  $z \sim \mathcal{N}(\mu + \Sigma g_{str}, \Sigma)$ , corresponding to the reported conclusion in Alg. 1. Note that all constants during the derivation could be safely ignored after computing the gradients. The process of LCDG is essentially sampling from a conditional Gaussian distribution, which could be approximated by a mean-shifted Gaussian distribution correlated with the structural condition.

Also, for DDIM sampling [20], the process could be formulated as:

$$\begin{aligned} \hat{\epsilon} &= \epsilon(z_t) + \sqrt{1 - \bar{\alpha}_t} \nabla_{z_t} \log p_\psi(\Delta\mathcal{C}|z_t), \\ z_{t-1} &= \sqrt{\bar{\alpha}_{t-1}} \left( \frac{z_t - \sqrt{1 - \bar{\alpha}_t} \hat{\epsilon}}{\sqrt{\bar{\alpha}_t}} \right) + \sqrt{1 - \bar{\alpha}_{t-1}} \hat{\epsilon}. \end{aligned} \quad (9)$$

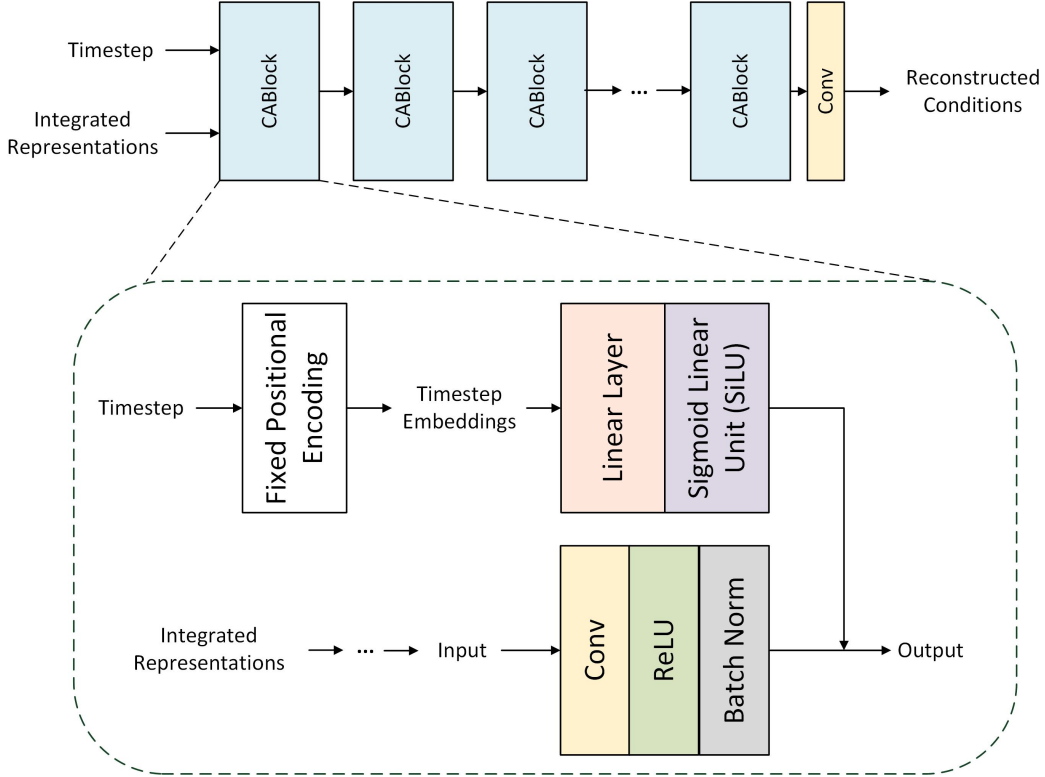


Figure 11: Graphical illustration of the network architecture of CA. The composed blocks of CA are denoted as CABlock.

Note that we add the conditional term instead of the original subtraction, since we re-write the estimated score during DDIM sampling in the form of negative gradients of  $\nabla_{z_t} \log p_\psi(\Delta\mathcal{C}|z_t)$ . Specifically, we implement LCDG together with classifier-free guidance [22]. Therefore, we write the sampling score at each step with [22] as:

$$\begin{aligned} \nabla_{z_t} \log p_\theta(z_t|c, C_{ext}) = & \underbrace{\omega \nabla_{z_t} \log p_\theta(z_t|c) + (1 - \omega) \nabla_{z_t} \log p_\theta(z_t)}_{\text{Classifier-Free Guidance}} \\ & + \underbrace{\beta \nabla_{z_t} \log \text{dist}(\mathcal{C}, C_{ext})}_{\text{Structure-Aware Diffusion Guidance}}, \end{aligned} \quad (10)$$

where  $t$  is the sampling timestep where  $t \in \{T, T - 1, \dots, T_{trunc}\}$ .  $T_{trunc}$  denotes the truncation threshold of TCS.  $c$  represents the text embeddings extracted by text encoders [46, 11].

## C Implementation Details

### C.1 Network architecture

Fig. 11 shows the detailed architecture design of CA. It is implemented with a series of CABlock, and a convolution layer at its end with kernel size of 1 for decreasing the channel size. Each CABlock has two-branch, which process timestep and the internal representations, respectively. For the timestep branch, the integer timestep is first implemented with a Positional Encoding (PE) same as those from the transformers [58], and extracted into timestep embeddings. The timestep embeddings are then sent into a linear layer and a Sigmoid Linear Unit (SiLU) sequentially, following the implementations of the one in diffusion U-Net [49]. On the other branch, the integrated representations pass through a simple architecture of Conv-ReLU-BN. The processed timestep embeddings are projected to the same shape as the intermediate features on the other branch. Then we finish the process of forwarding one block in CA by adding both of them. We implement the last layer of CA with solely a simple  $1 \times 1$  convolution instead of CABlock to downscale the channel size.

Table 2: Hyperparameter details of the proposed LCDG under different conditions for the evaluation upon COCO 2017 validation set [36].

	Ours (edge)	Ours (stroke)	Ours (palette)	Ours (mask)
SD version	1.4	1.4	1.4	1.4
DDIM steps	50	50	50	50
DDIM eta	0.0	0.0	0.0	0.0
Unconditional guidance scale	6	6	6	6
Controlling scale	2	2.5	2.5	2
Truncation threshold	500	650	750	600

## C.2 Data Preparation

As is mentioned in Sec. 4 in our main paper, we does not require annotated datasets to train the proposed LCDG, which indicates the flexibility of LCDG and its convenience to implement. We further illustrate the data preparation pipeline in details in this section. The collected dataset consists of 10,000 images. We use a pre-trained image captioning model [23] to automatically annotate the description for each image. We list details of the data preparation pipeline for each implemented condition as follows:

- *Edge conditions.* We use a HED-like edge detector [18] to detect the edge maps from the source images. To simulate Canny edge [7] during inference, we implement erosion operation upon the detected edge map in random degrees. To simulate user sketch, we implement dilation operation, random binarized threshold, random warping upon the detected edges. To detect Canny edge during inference, the binarize thresholds are set as 200 and 225.
- *Color stroke.* During training of CA, we select simulated color stroke as the supervision signal. We build our stroke simulation algorithm based on the one proposed in [39]. In practice, we first process the source image using a median filter with kernel size of 23. Then, we implement a k-means clustering upon the grayscale values of the filtered image, *i.e.*, color. For the centers of k-means clustering, we randomly sample  $k$  from  $\{4, 8, 12, 16\}$  during each simulation, to simulate different types of used color during interfaces. Note that we do not implement specific design for image palette. But it would be reasonable for LCDG to be compatible with image palette condition, which works as stroke of square shape and guides the overall color distribution. For simulation of image palette during inference, we first downsample the source image to  $8 \times 8$ , then upsample it back to the original resolution using the same nearest interpolation.
- *Mask conditions.* The binary mask condition is less investigated for the community of conditional image synthesis. Motivated by [24], we demonstrate some applications of practical usage with mask conditions in this paper. The mask condition provides a guidance of foreground position for diffusion sampling. Once precisely annotated, it also guides the contours of generated contents. The supervision signal of CA is simply the detected saliency mask using a pre-trained saliency detection model [45].

## C.3 Training Details

We provide the training details of the implementation of the proposed Condition Adapter (CA). To extract the internal representations of the diffusion models, we choose outputs of different layers in the diffusion U-Net, which include the 2th, 4th, 8th layers of the encoder, the last outputs of the middle layers, and outputs of the 2th, 4th, 8th, 12th layer of the decoder. We use L2 norm between the reconstructed condition and external condition for optimization, which corresponds to Eqn. 2 in our main paper. Besides, we use Adam [32] optimizer with learning rate of  $1 \times 10^{-4}$ . We train CA with 10,000 iterations, which requires approximately four hours of training on a single 3090 GPU. The batch size is set as 4.

## C.4 Evaluation Details

Tab. 2 and Tab. 3 provide the hyperparameter details of LCDG and other compared methods during the evaluation on COCO 2017 validation set [36]. We use the first caption of the official annotated

Table 3: Hyperparameter details of other compared methods for the evaluation upon COCO 2017 validation set [36]. We try to ensure all compared methods using the same diffusion backbone (SD v1.4) for fair comparison. Note that ControlNet [66] only implements their methods based upon SD [49] with version of 1.5.

	SD (text) [49]	ControlNet (edge)	SD* (stroke)	SD* (palette)	T2I (edge) [41]	T2I (stroke) [41]	T2I (palette) [41]
SD version	1.4	1.5	1.4	1.4	1.4	1.4	1.4
DDIM steps	50	50	50	50	50	50	50
DDIM eta	0.0	0.0	0.0	0.0	0.0	0.0	0.0
Unconditional guidance scale	7.5	9.0	7.5	7.5	7.5	9.0	9.0
Controlling scale (weight, strength)	-	1.0	0.8	0.8	1.0	1.0	1.0
$\tau_{\text{cond}}$	-	-	-	-	0.5	1.0	1.0

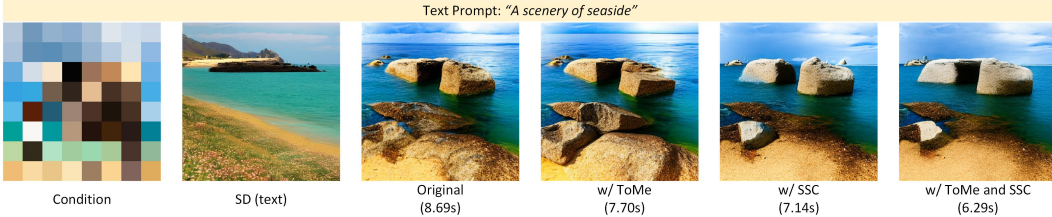


Figure 12: Qualitative results of LCDG using different acceleration strategies, including ToMe [4] and the proposed SSC strategy.

captions as corresponding text prompt following [41]. For fair comparison, we set the DDIM sampling steps as 50 for all compared methods. For simulation of HED edge [61], we use the HED detector [61] to detect edge maps from the source images. For stroke, palette, and mask conditions, we simulate these conditions the same as our introduction in Sec. C.2. For hyperparameter settings of ControlNet [66] and T2I-Adapter [41], we use the *recommended* settings (unconditional guidance scale for [22], controlling scale, and  $\tau_{\text{cond}}$  for [41]) following their official instructions according to different conditions. For the implementations of SD\* (SD using SDEdit [39]), we also follow the official *recommended* instructions of SD [49] with a controlling strength of 0.8.

## D Limitations

We illustrate and discuss some of the limitations and working boundaries of LCDG in this section. One aspect is that LCDG would increase the sampling time during inference. Such limitation is shared by gradient-based methods [14, 22] with additional forwarding processes of the diffusion U-Net. For LCDG during sampling, we require to pass the intermediate sample forward additionally to obtain the internal representations of the diffusion model.

Tab. 4 reports the sampling time compared with other methods. One could see that either early-constraint methods or the proposed late-constraint one would lead to certain degree of additional sampling time. This could be reasonable because introducing additional guidance into diffusion models require passing conditions through additional network components. Thus, all methods obtain slower sampling speed than text-to-image sampling of SD [49]. ControlNet [66] obtains the slowest sampling time, where the model parameters of ControlNet is approximately half of the diffusion U-Net of SD [49]. That is to say, at each sampling time, it requires to pass either the intermediate samples or the conditions through approximately 1.5 diffusion U-Net in total. T2I-Adapter [41] is the fastest of all, which requires passing through a additional condition-specific encoder at each sampling step. For LCDG, we need to pass  $z_t$  forward the diffusion U-Net and also the lightweight condition adapter at the manipulated steps using TCS.

We have also explored some possible solutions to alleviate such limitations. For LCDG, the main factor that determines the sampling time would be the truncation threshold in TCS, where the greater its value is, the less time we require to sample an image. To improve the sampling time, we implement ToMe [4] and a Skip-Step Conditioning (SSC) strategy to speed-up the original sampling process of LCDG. As for SSC strategy, we only manipulate even-numbered DDIM sampling steps within the TCS interval. Tab. 5 reports the sampling time with different truncation thresholds and the improved

Table 4: Sampling time compared to other methods, including SD [49], ControlNet [66], T2I-Adapter [41]. For LCDG, we assign the truncation threshold as 500 (maximum truncation magnitude of TCS). Note that the comparison is implemented with HED edge [61] as guidance on a single NVIDIA 3090 GPU.

	SD (text)	ControlNet	T2I-Adapter	Ours
DDIM steps	50	50	50	50
Sampling time	5.31	14.69	6.44	14.11

Table 5: Sampling time with different truncation thresholds, and with different acceleration strategies using ToMe [4] and SSC. DDIM steps is set as 50 and SD [49] with version of 1.4 is used as the base model. The sampling time is tested under the HED edge [61] as guidance on a NVIDIA 3090 GPU.

	Sampling Time
$T_{trunc} = 500$	14.11
$T_{trunc} = 600$	11.53
$T_{trunc} = 700$	10.04
$T_{trunc} = 800$	8.55
$T_{trunc} = 900$	7.02
$T_{trunc} = 500$ , using SSC	10.35
$T_{trunc} = 500$ , using ToMe (ratio=0.6)	11.21
$T_{trunc} = 500$ , using ToMe (ratio=0.6) and SSC	8.02



Figure 13: Qualitative results for the ablation studies of training data domains, implemented under HED edge [61] condition. We denote our reported experiment trained on self-collected data with synthetic labels from the internet as Random Set in this figure.

ones using the proposed solution. We notice that the accelerating effect of ToMe [4] would be more obvious while sampling images with higher resolution. Notably, we report the slowest sampling time in Tab. 4 with the most truncation magnitude. For other conditions which requires less manipulated steps to achieve the best performance, *e.g.*, image palette, it would be obviously faster than the reported one. Further, with the acceleration using ToMe [4] and SSC, we could obtain comparable sampling speed (6.29s) with the fastest one [41] (6.71s). Fig. 12 shows the corresponding qualitative results under the image palette condition, indicating that such acceleration strategy could produce satisfying results with acceptable details loss.

## E Extended Ablation Studies

### E.1 Training Data Domains

We ablate the effects of training CA with different specific domains of data, instead of randomly collected ones. Besides, we also ablate the effects of training CA with only simple class label or even no text prompt. We randomly collect a series of cats and dogs images from ImageNet [13], which consists of 10,400 images of 8 categories in total (class labels are: “*bernese mountain dog, french bull dog, old English sheep dog, maltese dog, siamese cat, tiger cat, egyptian cat, persian*”).

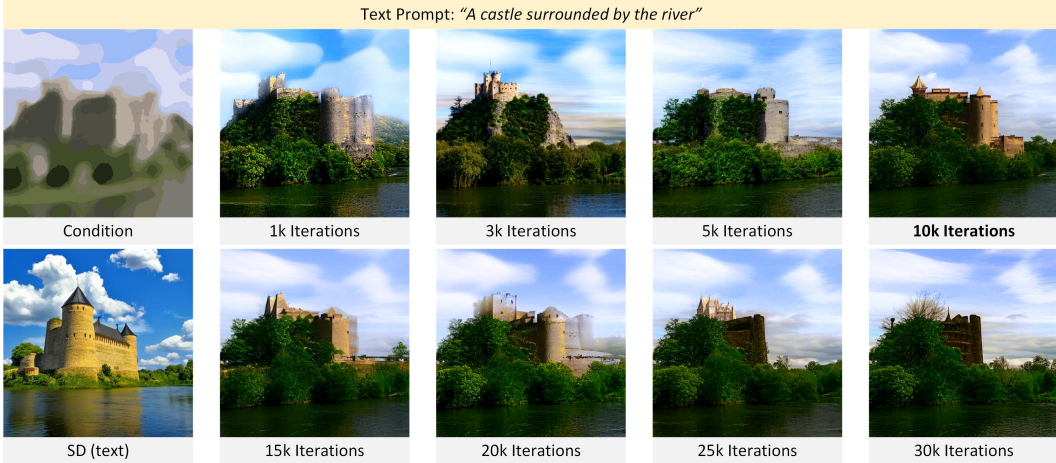


Figure 14: Qualitative results for the ablation studies of training iterations, implemented under color stroke condition. We highlight the model trained with 10k iterations as the **optimal** result.

*cat*”). We set the text prompts as “dog” for images with dogs, and “cat” for ones with cats. We also randomly collect 10,000 images from CelebA-HQ [27] as demonstration of the face domain. For the face domain, we simply use an empty string as text prompts.

Fig. 13 shows the qualitative results for the ablation studies. An interesting phenomenon is that training with solely face images even without text prompts could introduce the guidance of edge condition. However, the result is only approximately controlled with details loss, meanwhile revealing artifacts in the background. We regard this might be caused by the absence of text condition during the training of CA. The learned correlation fails to align with the text embeddings while sampling the text-to-image diffusion model, thus causing a inconsistency in the generated result. With simple class labels as text conditions, such phenomenon has been obviously alleviated with a better consistency with the text condition. The generated result embodies more detailed controls, *e.g.*, the pocket on the bag, but still obtaining artifacts. The experiments indicate that training with text conditions is still vital to ensure the performance of LCDG upon text-to-image diffusion models, but also address the potentials of implementing LCDG with more easy-collected data without salient text labels.

## E.2 Training Iterations

We further ablate the minimum training iterations of CA. Fig. 14 shows corresponding qualitative results. We demonstrate the ablation study under stroke condition for its complexity with three channels to learn than the binary conditions with only one. One could see that training with less than 10,000 iterations would be insufficient, where the guided results reveal unstable textures and artifacts. This indicates that CA fails to learn a promising correlation between the internal representations of diffusion and color condition. From results trained with more than 10,000 iterations, we could see that the contents are stable, but the overall color is darker and monotonous. An representative phenomenon is that the color of the castle is getting black, and the river reveals similar color as the forest. In such circumstances, CA is over-fitting the limited color distribution of the small-scale training data, and fails to generalize to more vivid color during inference. We recommend training with 10,000 iterations to obtain the best performance of LCDG.

## F More Qualitative Results

We demonstrate more qualitative results in this section. Sec. F.2 demonstrates qualitative comparison and corresponding analysis with state-of-the-art conditional image synthesis solutions, also denoted as *early-constraint* methods in this paper.

## F.1 More Conditional Text-to-Image Results with Unconditional Model

Fig. 15 and Fig. 16 report more results implemented under edge condition and color condition. Note that in each figure, we use the same model for evaluation.

## F.2 More Conditional Results with Text-to-Image Model

We provide more conditional text-to-image results compared with state-of-the-art competitors [49, 66, 41, 39] under each implemented condition separately, including Canny edge [7] (Fig. 17), HED edge [61] (Fig. 18), user sketch (Fig. 19), color stroke (Fig. 20), image palette (Fig. 21), segmentation mask (Fig. 22 left), and user scribble (Fig. 22 right). Notably, results in Fig. 17, 18, 19 share the same model. Results in Fig. 20, 21 use the same model. And all results in Fig. 22 are inferred with the same model, indicating the plausible generation ability of our method.

We analyze the inferred results from the following aspects:

1. **Qualitative Comparison.** One could see that the proposed LCDG could obtain outperforming results over other competitors [49, 66, 41, 39]. The generated results using LCDG are more consistent with the text condition, meanwhile following the guidance of external conditions. *Early-constraint* methods, however, could sometimes be not consistent with the text condition due to the provided internal regularization, *e.g.*, the generated result in Fig. 17 using [41] fails to generate a church under the blue sky. In reverse, the *late-constraint* manner of LCDG is compatible with the original text-to-image sampling, thus producing more consistent results.
2. **Cross Evaluation of Early-Constraint Methods.** In the reported results, we also prove our observation that *early-constraint* methods obtain poor generalization ability to other conditions. Since T2I-Adapter [41] only implement their method under sketch condition, the evaluated performance upon HED edge is less satisfying. For instance, the generated results could sometimes fail to produce consistent results with the text condition, *e.g.*, the generated forest behind the blimp instead of the prompted “sky”. For color condition, SD\* is implemented for the stroke condition, and T2I-Adapter [41] is designed for color palette. For a cross evaluation, we also evaluate their performance on image palette and color stroke, respectively. For color stroke, results generated by [41] reveal severe color discrepancy. Also, SD\* [49] tends to produce blur and less detailed results due to the failure of generalizing to the palette guidance.
3. **Structural Guidance Benefits Sample Quality.** We observe that most of the guided results using LCDG are more qualitatively satisfying than the text-driven ones generated by SD [49]. Taking mask-guided results as examples, one could see that the manipulated results are in better quality in most cases. This corresponds to the analysis of Fig. 3 and Tab. 1 in our main paper, where the visualized structures of intermediate samples during text-to-image diffusion sampling are unstable and in disorderliness. Even with user scribble of a few strokes, the guided results are more plausible than the text-to-image ones, demonstrating the effectiveness of the proposed diffusion guidance in the *late-constraint* manner.

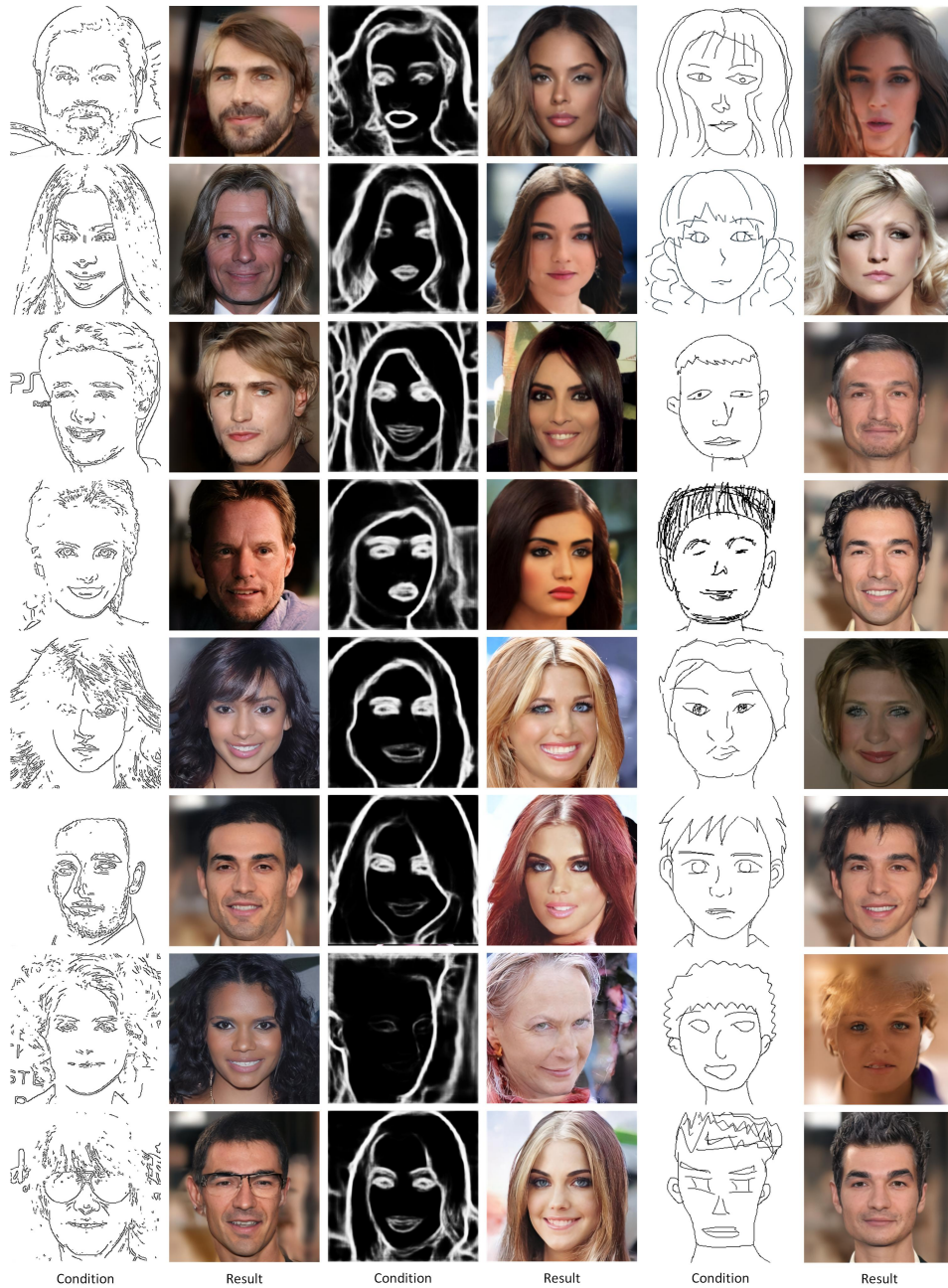


Figure 15: More results under edge condition working with SD [49] trained on CelebA-HQ [27], including Canny edge [7], HED edge [61], and user sketch (from left to right). Note that the sketches are collected from the released free-hand sketches of [63].

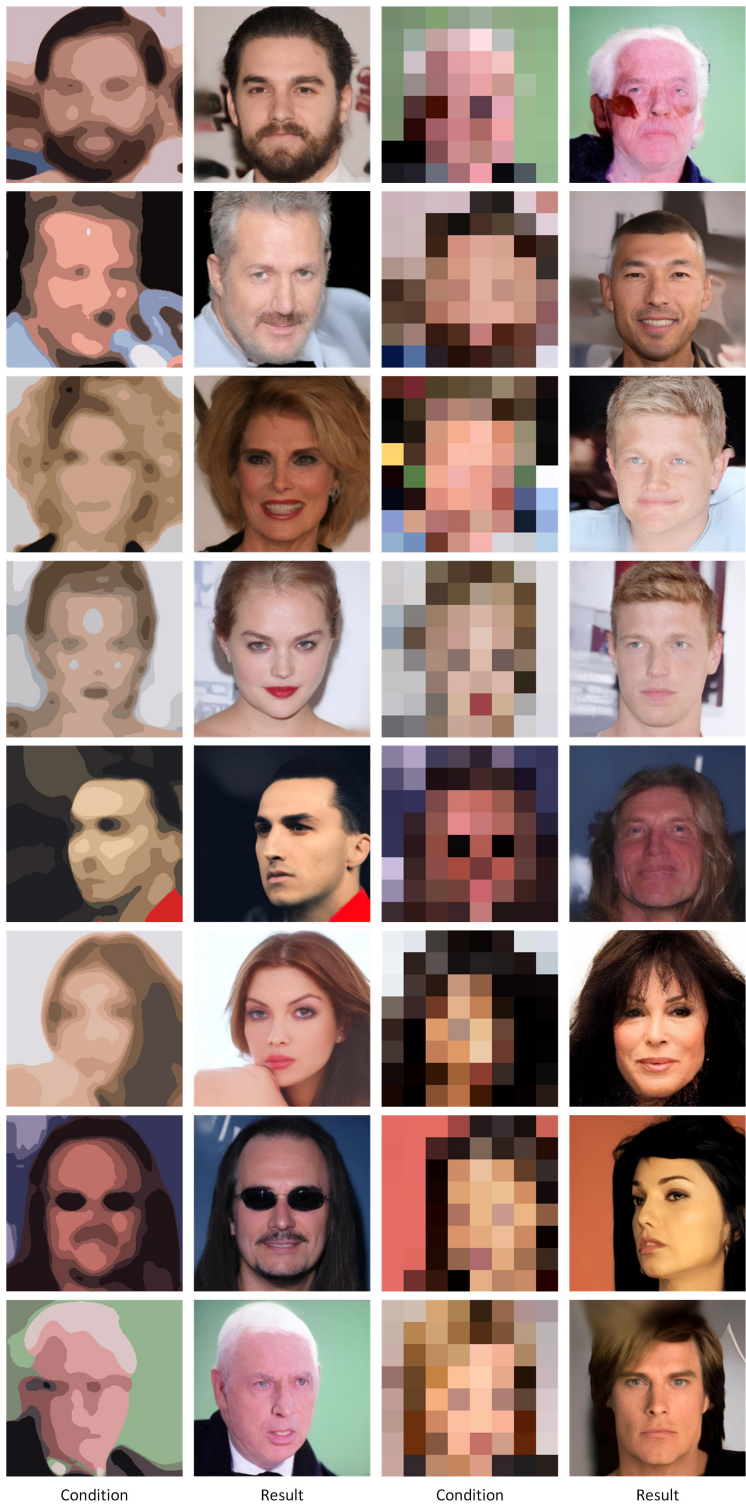


Figure 16: More results under color condition working with SD [49] trained on CelebA-HQ [27], including color stroke (left) and image palette (right).



Figure 17: More results and comparison of Canny edge [7] condition working with text-to-image SD [49], compared to ControlNet [66], and T2I-Adapter [41]. We also evaluate the result of text-to-image SD [49] for reference in this figure.

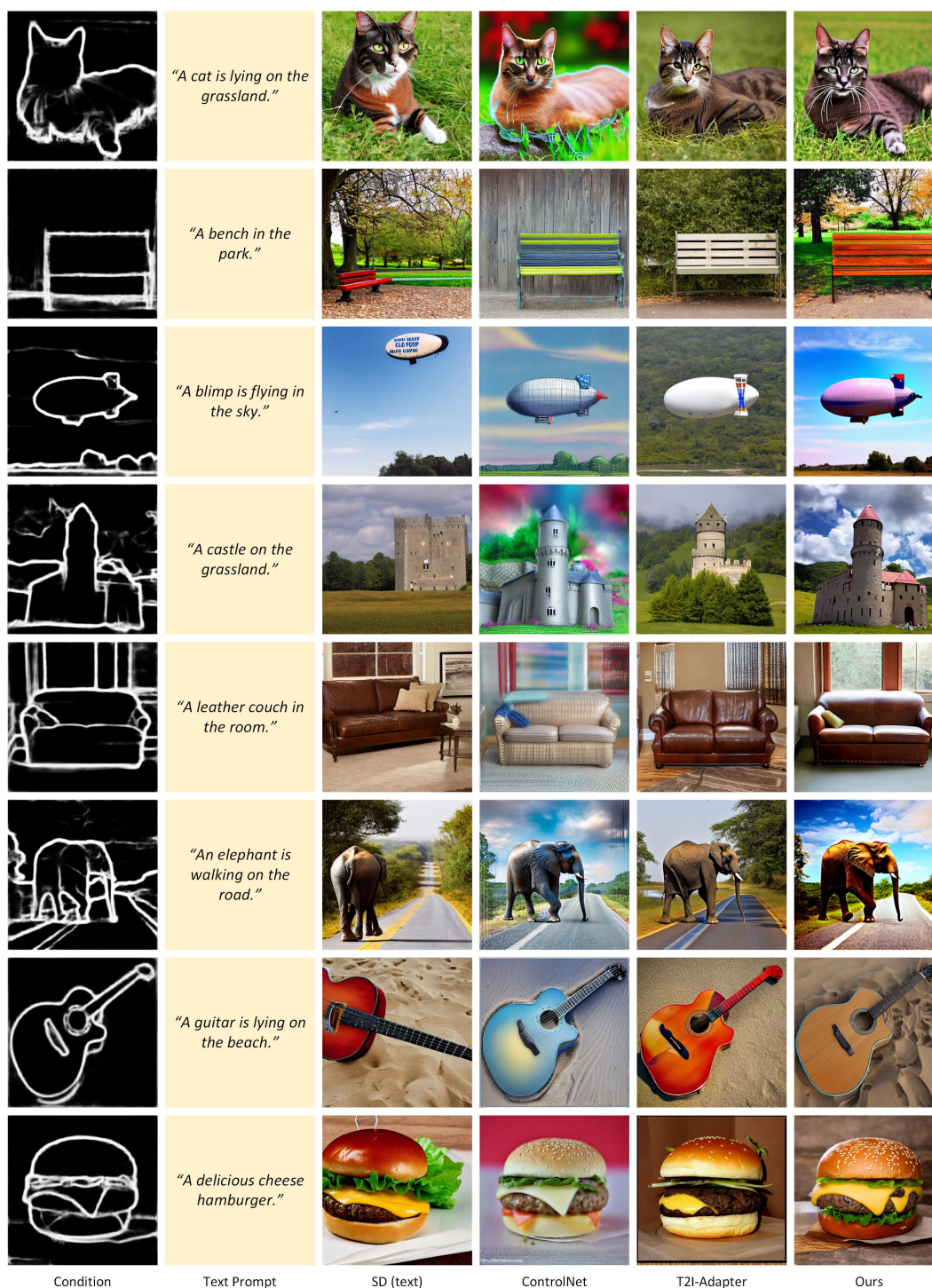


Figure 18: More results and comparison of HED edge [61] condition working with text-to-image SD [49], compared to ControlNet [66], and T2I-Adapter [41]. We also evaluate the result of text-to-image SD [49] for reference in this figure. Since T2I-Adapter [41] does not implement an individual model for HED edge condition, we use their released sketch model for evaluation.

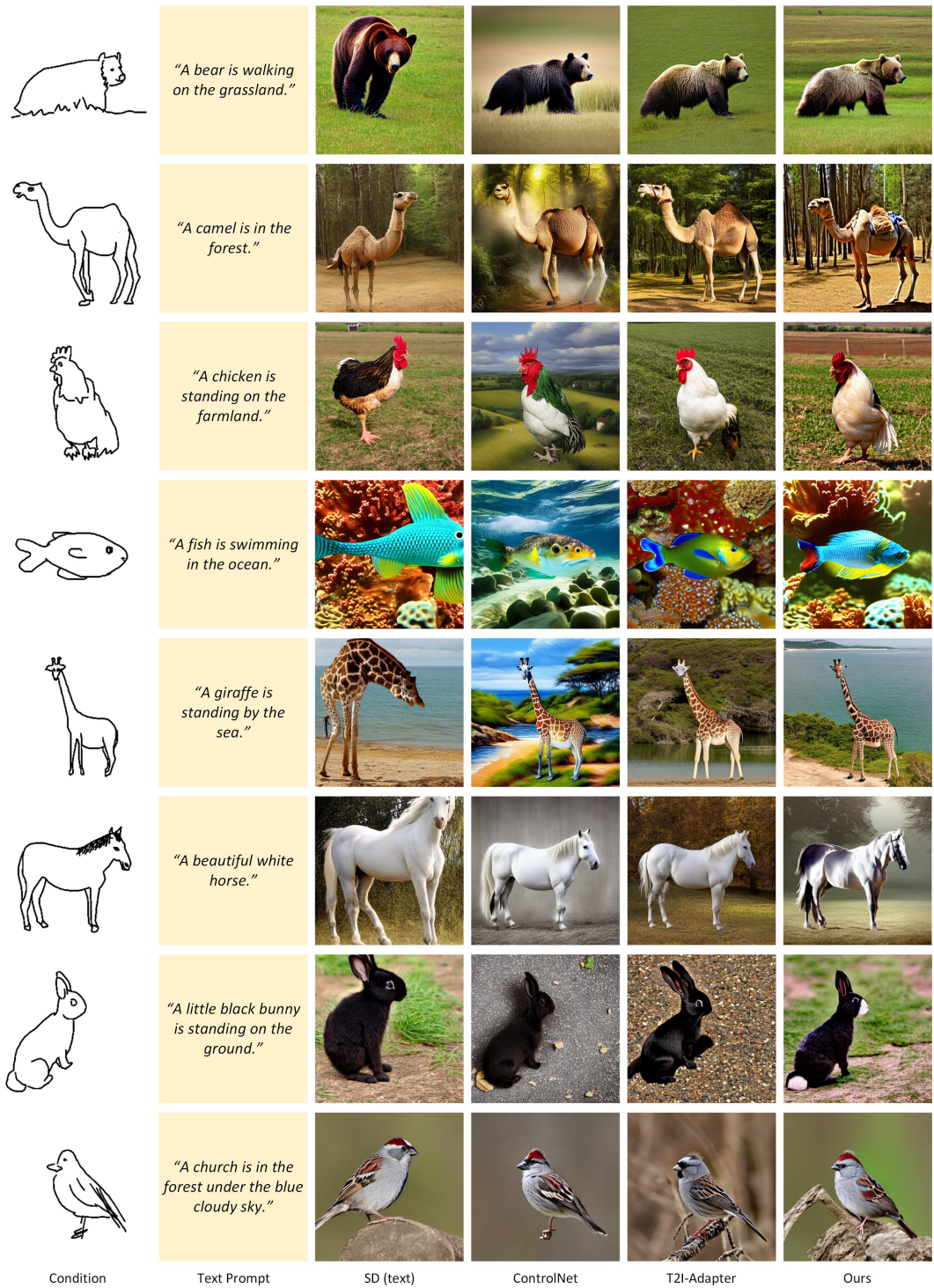


Figure 19: More results and comparison of user sketch condition working with text-to-image SD [49], compared to ControlNet [66], and T2I-Adapter [41]. We also evaluate the result of text-to-image SD [49] for reference in this figure. Note that the sketches are collected from Sketchy [53] dataset.

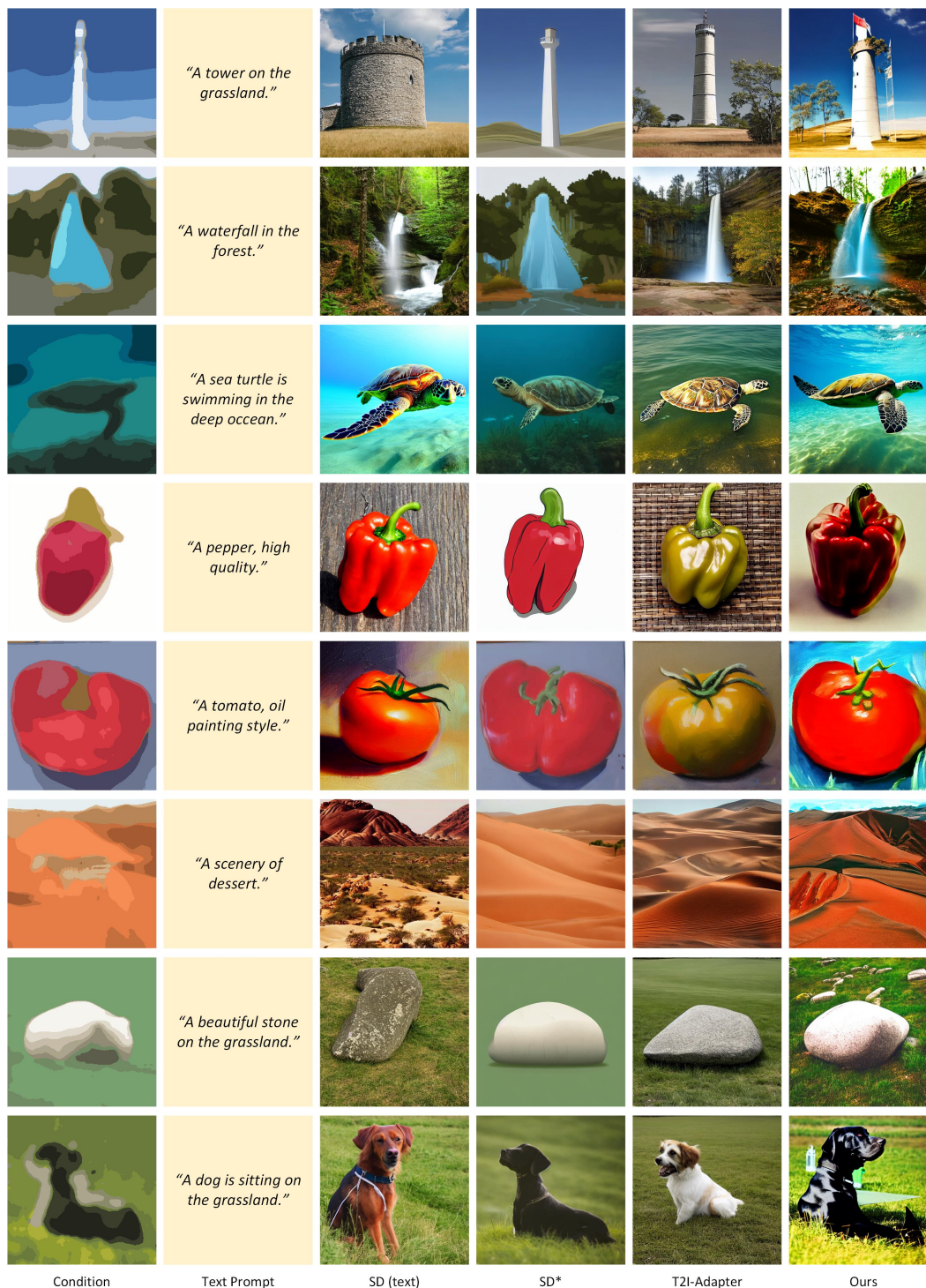


Figure 20: More results and comparison of color stroke condition working with text-to-image SD [49], compared to SD\* (SD using SDEdit [39]) and T2I-Adapter [41]. We also evaluate the result of text-to-image SD [49] for reference in this figure. Since T2I-Adapter [41] does not implement an individual model for color stroke condition, we use their released color model for evaluation.

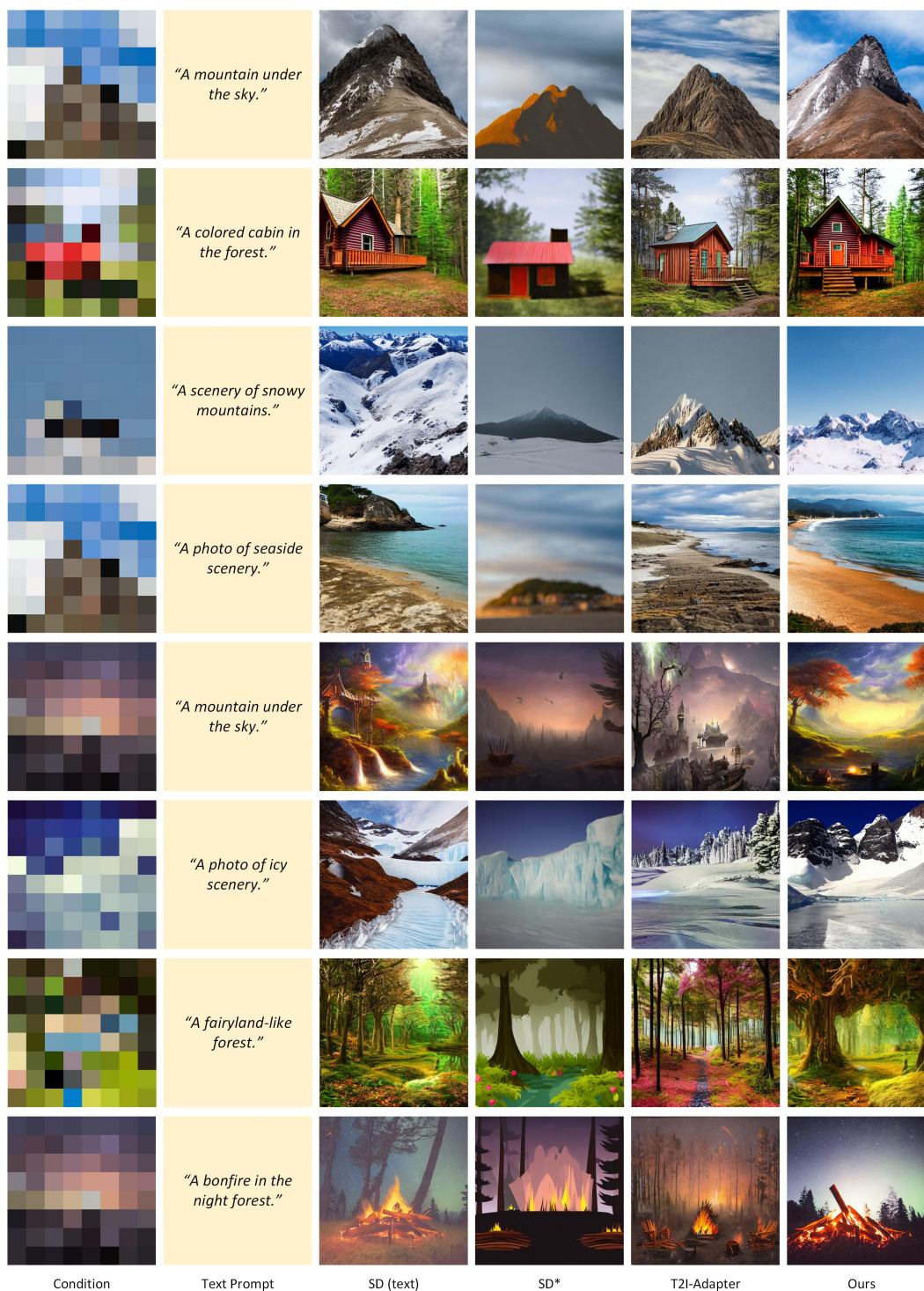


Figure 21: More results and comparison of image palette condition working with text-to-image SD [49], compared to SD\* (SD using SDEdit [39]) and T2I-Adapter [41]. We also evaluate the result of text-to-image SD [49] for reference in this figure, and further evaluate SD\* [49] in this figure for a cross evaluation of its performance upon unseen condition, *i.e.*, image palette.

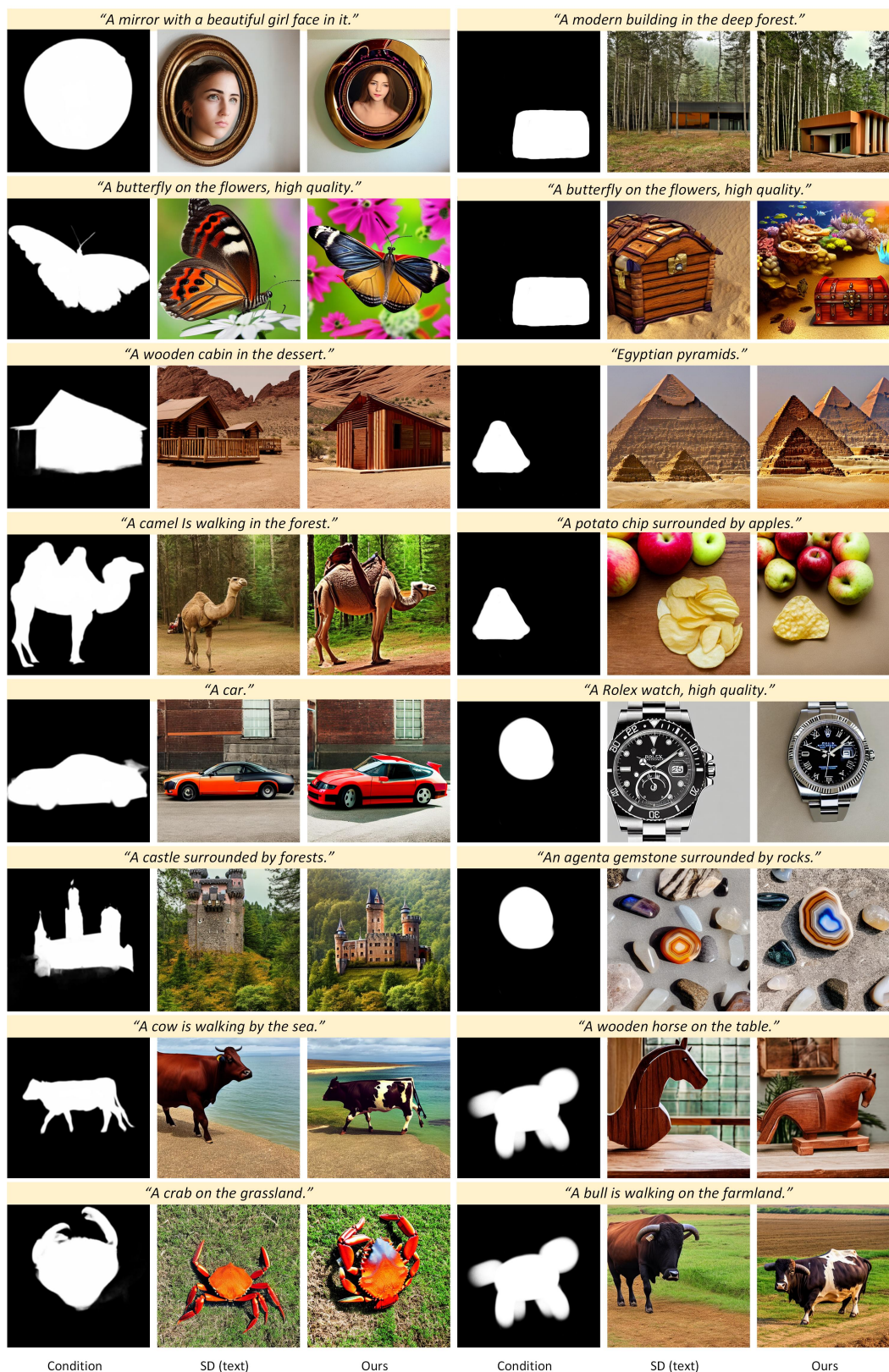


Figure 22: More results of segmentation masks (left) and user scribble (right) working with text-to-image SD [49].